PNAS
www.pnas.org

Main Manuscript for

Persulfidation of ATG18a regulates autophagy under ER stress in Arabidopsis.

Angeles Aroca [1,2 *], Inmaculada Yruela [3,4], Cecilia Gotor [2], Diane C. Bassham[1]

[1] Department of Genetics, Development and Cell Biology, Iowa State University, Ames, Iowa USA.

[2] Institute of Plant Biochemistry and Photosynthesis, University of Seville and CSIC, Seville, Spain.

[3] Estación Experimental de Aula Dei, Consejo Superior de Investigaciones Científicas, Zaragoza, Spain.

[4] Group of Biochemistry, Biophysics and Computational Biology (BIFI-Unizar) Joint Unit to CSIC, Spain.

*Angeles Aroca

Email: aaroca@us.es

Author Contributions: A.A. designed and performed research, analyzed the data and wrote the article. I.Y. performed 3D protein modeling research and analyzed the data, C.G. contributed to writing and reviewing the manuscript, D.C.B contributed to designing research, writing and reviewing the manuscript. All authors contributed to the discussion.

Competing Interest Statement: The authors declare no competing interest.

Classifications: Biological Science. Plant Biology

Keywords: autophagy, hydrogen sulfide, ER stress, ATG18a, persulfidation.

.

This PDF file includes:

Main Text
Figures 1 to 6

Significance Statement

Endoplasmic reticulum stress is a condition triggered by adverse environmental conditions, which in plants include extreme heat, pathogen infection and drought. These stresses can have

a devastating effect on agricultural productivity, and the appropriate responses of plants to stress are therefore critical. Autophagy is a macromolecular degradation pathway that is activated in response to stress, including ER stress, but the mechanism by which it is regulated is still unclear. Here we describe a novel modification, persulfidation, of the key autophagy protein ATG18a that affects its binding to membranes and controls its activity. This tight regulation of autophagy therefore allows plants to control the tradeoff between growth and stress tolerance.

Abstract

Hydrogen sulfide (H_2S) is an endogenously generated gaseous signalling molecule, which recently has been implicated in autophagy regulation in both plants and mammals through persulfidation of specific targets. Persulfidation has been suggested as the molecular mechanism through which sulfide regulates autophagy in plant cells. ATG18a is a core autophagy component that is required for bulk autophagy and also for reticulophagy during ER stress. In this research, we have revealed the role of sulfide in plant ER stress responses as a negative regulator of autophagy. We demonstrate that sulfide regulates ATG18a phospholipid-binding activity by reversible persulfidation at Cys103, and this modification activates ATG18a binding capacity to specific phospholipids in a reversible manner. Our findings strongly suggest that persulfidation of ATG18a at C103 regulates autophagy under ER stress and the impairment of persulfidation affects both the number and size of autophagosomes.

Main Text

Introduction

Macroautophagy (hereafter autophagy, from the Greek meaning 'self-eating') is a major catabolic process in eukaryotic cells to degrade dysfunctional or unnecessary cellular components, either non selectively or selectively (1, 2). It has conserved functions in development, cellular homeostasis, and stress responses from yeast to plants and mammals. In plants, autophagy is critically important in many aspects of plant life, including seedling establishment, development, stress resistance, metabolism and reproduction (1). The autophagy mechanism involves the enclosure of a portion of the cytoplasm into a double membrane vesicle, named an autophagosome. The outer membrane of the autophagosome finally fuses with the vacuole (in yeast and plants) to release the inner autophagic body for hydrolytic degradation of the sequestered cargo. About 40 *ATG* (autophagy-related) genes have been identified in Arabidopsis, which are required for autophagosome formation (3). Autophagy was initially characterized as a bulk degradation pathway induced by nutrient deprivation with a role in nutrient recycling to enable cell survival, but it also contributes to intracellular homeostasis by selectively degrading aggregated proteins, damaged mitochondria, ribosomes, toxic macromolecules, excess peroxisomes, and pathogens to prevent toxicity (4-6). In particular, although the endoplasmic reticulum (ER) is involved in autophagic processes as a source for membranes, it is also the target of a selective type of autophagy, termed reticulophagy or ER-phagy. In plants, this ER-phagy is induced in response to ER-stress produced by tunicamycin or DTT treatments (7) and upon starvation(8). Selective autophagy is mediated by the binding of adaptor proteins, which link a cargo targeted for degradation to the autophagosome machinery (9). These selective autophagy receptors share the feature of interacting with the autophagosome-localized protein ATG8 through an ATG8-interacting motif (AIM) or an ubiquitin-interacting motif (UIM), leading to their recruitment into forming autophagosomes (10-12).

An increasing number of targets for selective autophagy under different stress conditions have emerged in recent years, but the underlying mechanisms of regulation of their degradation are still so far unknown. The activation of bulk and selective autophagy must be tightly controlled by the cellular conditions. In that sense, ATG4 is the only ATG that has been shown to be redox regulated in animal, yeast, algae and plant systems (13-18). Nevertheless, in the last decade, a growing number of targets involved in autophagy have been shown to be regulated by different posttranslational modifications (PTMs); for example, ATG4b and ATG1 are regulated by *S*-nitrosylation and phosphorylation (19, 20). Therefore, the ability of the ATG proteins to interact with a number of autophagic regulators is modulated by different PTMs such as phosphorylation, glycosylation, ubiquitination and nitrosylation (21).

Protein persulfidation is another player in the redox regulation of certain proteins. It is the mechanism for sulfide-mediated signaling, and is an oxidative posttranslational modification of cysteine residues caused by hydrogen sulfide (H_2S) in which thiolate (–SH) is transformed to a persulfide group (–SSH). Persulfidation of proteins can affect their function, localization inside the cells, stability, and resistance to oxidative stress (22-27). H_2S is an endogenously generated gaseous signaling molecule, which has been recently implicated in autophagy regulation both in plants and mammals (28-30).

Analysis of the Arabidopsis *des1* mutant, impaired in the cytosolic production of H_2S from cysteine, led to the conclusion that H_2S acts as an inhibitor of autophagy induced by nutrient deprivation (28). Interestingly, its action is independent of ROS and nitrogen starvation and the mechanism of autophagy inhibition by H_2S has been proposed to be through persulfidation of specific targets (31). Recently, regulation of the proteolytic activity of ATG4 by persulfidation has been demonstrated in plants (16). Autophagy induced upon nitrogen starvation or osmotic stress was negatively regulated by sulfide, and the mechanism has been explained through persulfidation of C170 of this ATG4 protease, which inhibits proteolytic activity. Collectively these results suggest that persulfidation may be the molecular mechanism through which sulfide regulates autophagy in plant cells. The susceptibility to persulfidation of the additional autophagy (ATG)-related proteins ATG18a, ATG3, ATG5, and ATG7 was revealed using a high throughput proteomic approach (32), although the role of this modification in these other ATG proteins has not yet been revealed. ATG18a is a core autophagy protein that binds to phosphoinositides (33, 34). It has a 7-bladed β-propeller structure, formed by WD40 repeats that bind phosphatidylinositol 3-phosphate (PtdIns(3)P) or phosphatidylinositol (3,5)-bisphosphate (PtdIns(3,5)P2). These two phosphoinositide binding sites are located in blades 5 and 6 surrounding and sandwiching the conserved L/FRRG motif. ATG18a forms a complex with ATG2 which is involved in autophagosome biogenesis during phagophore expansion (34), involved in the formation of pre-autophagosomal structures and lipid recruitment. ATG18a is essential for autophagy under several abiotic stresses and (RNAi)-*ATG18a* transgenic plants showed an autophagy-defective phenotype during nutrient stress and senescence (35, 36). *atg18* mutants show defects in autophagosome formation and display an early senescence phenotype (34). In addition, the ER is a target of autophagy during ER stress in plants, and this ER stress-induced autophagy is dependent on the function of ATG18a (37). Thus, ATG18a is likely to be required for autophagosome formation in Arabidopsis for bulk autophagy, and also for reticulophagy during ER stress (37) .

In this study, we aimed to clarify the role of sulfide in the regulation of autophagy under ER stress, through persulfidation of ATG18a. We found that persulfidation affects ATG18a lipid binding activity, which in turns regulates the number and size of autophagosomes produced upon ER stress.

Results

Persulfidation of ATG18a occurs at C103 and is sulfide-concentration-dependent.

We showed previously in a proteome-scale analysis that Arabidopsis ATG18a is a target for persulfidation (32). To elucidate the target site for persulfidation in ATG18a we carried out liquid chromatography (LC)-tandem mass spectrometry (MS/MS) analysis on the recombinant purified ATG18a protein. Protein was purified from an *E.coli* extract and trypsin digested under non-reducing conditions to avoid the reduction of persulfide residues. As disulfide bridges between digested peptides cannot be avoided, 2 missed cleavages were allowed in the search. The digested peptides were analyzed using LC-MS/MS for a 32-Da mass increase plus carbamidomethylation (SS-CAM) in the fragmentation spectrum. ATG18a was identified with a sequence coverage of 79% (Figure 1A), and the only peptide showing SS-CAM modification was ILNCDPFR, showing C103 with a persulfide modification (Figure 1B). The XCorr value from the search with the SEAQUEST engine for the $ILNC_{(SS\text{-}CAM)}DPFR$ peptide was 2.59. All of the other seven Cys residues were identified in the analysis, but none of them were modified by persulfidation.

To determine whether the modification was sulfide-dose dependent, an in-gel detection of persulfidated ATG18a protein was performed. Purified recombinant GST-ATG18a was incubated with increasing concentrations (100 nM-200 µM) of the sulfide donors NaHS and Na_2S_4, and with two reducing agents TCEP and DTT. A newly described dimedone switch detection method was then used (38), where NBF-Cl reacts with all Cys residues and amino groups giving a characteristic fluorescence (λex=488 nm) (39); and then persulfide adducts were selectively labelled with Daz-2/Cy5-alkyne

(Figure 1C). Results showed that higher concentrations of either NaHS or Na_2S_4 produced a more intense Cy5-fluorescent band as a result of a higher level of persulfidation in ATG18a (Figure 1D-E). Band quantification demonstrated that protein treated with either sulfide donor at concentrations as low as 1 µM showed a significant increase in protein persulfidation in comparison with untreated protein. Reducing agents efficiently reduced the intensity of the Cy5-fluorescent band, indicating a decrease in ATG18a persulfidation levels when treated with DTT or TCEP. This shows that persulfidation of ATG18a protein is a reversible modification. Free GST protein was used as negative control to test whether persulfidation of ATG18a was affected by GST persulfidation (Suppl. Fig. 1A), and although a band was observed indicating persulfidation, it was not Na_2S_4 dose dependent. Furthermore, no persulfidated peptides from GST were identified by mass-spectrometry. Additionally, no persulfidated band was observed in the mutant purified recombinant ATG18a_C103S (Suppl. Fig. 1B).

ER-stress-induced autophagy is negatively regulated by sulfide

ATG18a has been shown to be critical for ER stress-induced autophagy in Arabidopsis (37). The effect of sulfide on autophagy regulation was therefore tested under ER stress. Arabidopsis transgenic seedlings expressing GFP-ATG8e were treated with TM to induce ER-stress and with sulfide to test its role. Numerous autophagosomes were visualized after TM treatment in comparison with the control, where the autophagosomes were very few (Figure 2A). The number of autophagosomes in the root per frame was quantified manually, and roots treated with TM showed significantly more autophagosomes compared with control roots (Figure 2B). Treatment with sulfide had no significant effect on the number of autophagosomes in the absence of ER stress. By contrast, seedlings treated with TM and sulfide showed a drastic decrease in number of autophagosomes compared with TM alone. ER-stress can be alleviated by antioxidant treatments (40) and sulfide is able to increase the antioxidant capacity of the cell by inducing the activity of several antioxidant proteins (25, 41, 42). To test if the effect observed was due to the oxidative stress alleviation, treatments with ascorbic acid and glutathione were performed. Compared with control conditions, no effect was observed when treatments were applied under non-stress conditions. In addition, when ER-stress was induced with TM, no significant decrease in autophagosomes was detected upon ascorbic acid or glutathione treatments, indicating that the effect of sulfide is not due to its antioxidant properties.

Another approach was performed in order to corroborate these observations. WT or GFP-ATG8e-expressing seedlings were treated with TM for 6 hours and for a prolonged period of 12 and 24 h, and treated with sulfide for 1 hour. The effect of sulfide on autophagy was analyzed by quantification of the autophagy marker ATG8 protein by immunoblot using anti-ATG8 antibody (Figure 2C) or by analysis of GFP-ATG8e cleavage (Suppl. Fig.2A). Results showed that seedlings incubated with TM induced autophagy with the highest level of induction ranging from 12 to 24 h of treatment; meanwhile those treated together with sulfide showed a decrease in autophagy induction reaching similar levels as observed in the absence of TM (Figure 2C, Suppl. Fig.2A).

These data suggest that autophagy induced under ER-stress is negatively regulated by sulfide, to a much greater extent than by antioxidant treatments.

It was shown previously that the ER is degraded by autophagy during ER stress in Arabidopsis (37). Therefore, we studied the effect of sulfide on ER degradation using the fluorescent ER marker protein, GFP-HDEL, under ER stress conditions (43). Confocal microscopy showed the typical ER networks in the cytoplasm in control treatments. Similarly, in the presence of 1 µM concanamycin A (conA) to prevent vacuolar degradation, the vacuole lacked GFP fluorescence in control samples (Figure 3, Suppl. Fig. 3A). Accumulation of endogenous ATG8 was observed in GFP-HDEL plants treated with TM, while when plants were treated with TM and sulfide no differences were observed in comparison with control (Suppl. Fig. 3B-C). Similar results were observed in plants treated with sulfide. When plants were treated with TM, a clear increase in GFP-HDEL ER-labelling was observed in the vacuole after conA incubation, demonstrating that ER was being degraded in the vacuole. However, plants treated with both TM and sulfide lacked the increase in fluorescence in the vacuoles, showing ER localization similar to the control treatments. To confirm that TM was causing ER stress and that the sulfide does not prevent or alleviate the ER stress, but on the contrary regulates autophagy-specific ER degradation, we assessed bZIP60 splicing in plants treated with TM and sulfide for 6, 12 and 24 h. bZIP60 is an ER stress-responsive transcription factor that is spliced only upon ER stress (44), and

the splicing event can be detected by PCR. The results showed that sulfide did not alleviate ER stress, suggesting that the effect observed was specific for autophagy; although ER stress was persistent, autophagy was blocked (Suppl. Fig. 2B). Collectively, these results suggest that ER degradation by autophagy is regulated by sulfide.

Sulfide enhances ATG18a binding to membranes

Atg18 protein from *Saccharomyces cerevisiae* and WIPI3 and WIPI4 from mammals are homologues of ATG18a and they were reported to bind to PtdIns(3)P and PtdIns(3,5)P_2 (33, 45-47). The role of sulfide in the phosphoinositide-binding activity of ATG18a protein was assayed using PIP strips. PIP strips contain 100 pmol of 15 different lipids (Figure 4A) spotted onto a cellulose blotting membrane and protein-lipid binding specificity can be analysed easily.

To determine the role of persulfidation in the binding activity of ATG18a, recombinant GST-ATG18a protein was preincubated with increasing concentrations of Na_2S_4 and TCEP and then subjected to PIP strip binding. Results showed that untreated protein had specificity for PtdIns(3)P, and a weaker binding to PtdIns(3,5)P_2 was observed (Figure 4B-C). Sulfide enhanced the binding activity to both phosphoinositides, although more specifically to PtdIns(3)P. Binding was sulfide-dose dependent and treatment with 100 µM Na_2S_4 caused a substantial increase in binding. Treatment with TCEP significantly decreased binding to both phospholipids, demonstrating the reversibility of the sulfide induction of the ATG18a binding activity. Binding of the mutant recombinant protein GST-ATG18a_C103S was also assessed. Both untreated and sulfide treated protein showed a very significantly reduced binding to these phosphoinositides in comparison with the wild-type protein (Figure 4D-E). Free GST protein was assayed in PIP strips to corroborate that the tag did not affect binding in the recombinant proteins, and results showed that GST had no PtdIns(3)P -binding ability (Suppl. Fig. 4). These results suggested that the binding of ATG18a to PtdIns(3)P is significantly and reversibly increased by persulfidation. In addition, a weaker affinity toward PtdIns(3,5)P_2 was observed, although the effect of sulfide on this binding is inconclusive.

To confirm this effect *in vivo, Δatg18a* YFP-ATG18a_WT and Δ*atg18a* YFP-ATG18a_C103S seedlings were treated with TM and sulfide and a whole protein extract was subjected to cellular fractionation, to separate cytosolic proteins and the membrane-bound fraction. The level of enrichment of cellular fractionation was checked using specific markers for membranes (anti-H^+ATPase) and cytosol (anti-OASA-1) (Suppl. Fig. 5), Treatment with TM increased the level of YFP-ATG18a_WT in comparison with untreated seedlings, and furthermore, the proportion of YFP-ATG18a_WT protein in the membrane-bound fraction was significantly higher in seedlings treated with TM and sulfide than in those treated with only TM (Figure 4F-G). This suggests that sulfide treatment increases the proportion of YFP-ATG18a_WT in the membrane fraction. This effect was not observed with the mutant version of the protein, YFP-ATG18a_C103S, where the proportion of bound protein to membrane was even lower than the control or the TM treated sample. These *in vitro* and *in vivo* experiments suggest that sulfide enhances ATG18a binding to membranes by persulfidation of the C103 residue.

Sulfide regulates autophagosome biogenesis by persulfidation of ATG18a during ER stress

To further examine the subcellular localization of ATG18a and ATG18a_C103S in the plant cell, and to test their colocalization with ATG8e and therefore with autophagosomes and their precursors, we generated transgenic plants coexpressing YFP-ATG18a_WT or YFP-ATG18a_C103S and Cerulean-ATG8e in a Δ*atg18a* background. These seedlings were treated with TM and sulfide to study the effect of sulfide during ER stress. By confocal microscopy, ATG18a and ATG8e colocalized, but colocalization time was significantly shorter in those seedlings with the mutant version of ATG18a (Figure 5A, Suppl. Fig. 6). YFP-ATG18a_WT seedlings showed a YFP/CFP colocalization mean time of 66 seconds while for YFP-ATG18a_C103S it was 24 seconds. Surprisingly, treatments with TM or sulfide did not affect the YFP/Cer colocalization time in comparison with their respective control (Figure 5B). The shortening in the colocalization time of ATG8e and the mutated version of ATG18a could be indicative of the involvement of C103 of ATG18a in autophagosome biogenesis. To assess whether the mutation in C103 alters the number or size of autophagosomes, we measured these parameters for ATG8-positive puncta within the cells of YFP-ATG18a_WT and YFP-ATG18a_C103S seedlings

coexpressing Cer-ATG8e. Average size was measured for *n*>200 puncta over three independent experiments for each condition using ImageJ (48). Results showed that the mutated version of ATG18a decreased the size of autophagosomes compared with the WT version (Figure 5C-D, Supp. Fig. 7), suggesting that the impairment of ATG18a for persulfidation could affect the average size of autophagosomes. Furthermore, as expected, YFP-ATG18a_WT seedlings showed an increase in Cer-ATG8e puncta number when treated with TM, which was reverted after sulfide treatment (Figure 5E). However, untreated YFP-ATG18a_C103S seedlings showed an increase in autophagosome number in comparison with YFP-ATG18a_WT, which was even higher upon treatment with TM. However, sulfide treatment had no significant effect on the number of puncta in YFP-ATG18a_C103S seedlings under ER stress, with no decrease seen. To confirm the effect of YFP-ATG18a_C103S on the extent of autophagy in comparison with YFP-ATG18a_WT, ATG8 levels were measured by immunoblot assay. Results showed that YFP-ATG18a_C103S seedlings had increased levels of ATG8 compared with WT in control conditions (Suppl. Fig. 8 A-B). In addition, TM treatment increased ATG8 levels in both genotypes but sulfide treatment was only able to decrease ATG8 levels in YFP-ATG18a_WT seedlings. Furthermore, autophagy flux was measured under nitrogen starvation stress in both genotypes, and results showed that ATG8 levels were in general higher in YFP-ATG18a_C103S than YFP-ATG18a_WT while the ratio free CFP/CFP-ATG8 was smaller in YFP-ATG18a_C103S (Suppl. Fig. 8 C-D). However, under this stress condition, C103S mutation on ATG18a did not affect the negative regulation of autophagy by sulfide. These results suggest that persulfidation of ATG18a at C103 regulates autophagy under ER stress, but no under nitrogen starvation, and the impairment of persulfidation affects both the number and size of autophagosomes.

Persulfidation of ATG18a affects the cavity containing C103 and the surrounding electrostatic interaction network

To examine the impact of the persulfidation posttranslational modification of C103 in the interaction between AtATG18a and phosphoinositide molecules we have performed 3D homology modelling and structural alignment using the *Homo sapiens* HsWIPI3 – ATG2A:WIR peptide complex (49). AtATG18a shares up to 43.95 % sequence identity with HsWIPI3 (E-value 2.3x10-32), with conserved residues covering the full sequence. In particular, two highly conserved but not identical phosphoinositide-binding sites (site I and site II), and the potential lipid binding site III (47) are shown (Figure 6A). The 3D structural alignment revealed the lack of a β-sheet and the presence of a long flexible extension in AtATG18a compared with HsWIPI3 (Figure 6A). This long flexible loop is negatively charged and likely affects the charge distribution around binding-site I compared with HsWIPI3 (Suppl. Fig. 9). This finding might negatively influence the binding of PtdIns(3,5)P_2 to AtATG18a site I, explaining the weaker binding observed (Figure 4). It is worth mentioning that site I and site II differ in lipid affinity. Site I tends to recognize preferentially PtdIns(3,5)P_2 whereas site II interacts with PtdIns(3)P (47).

The residue C103 is located inside a hydrophobic cavity formed by residues ^{83}FNQD^{86} and F90 which are highly conserved in the WIPI members of the PROPPIN protein family (49). In fact, these residues of AtATG18a are at the exact positions of those of human WIPI3 (Figure 6A inset). Studies in the homologues WIPI4 and WIPI3 have demonstrated that the equivalent residues N15/N19, and D17/D21, respectively, to N84 and D86 of AtATG18a are essential for ATG2A binding (49, 50). Interestingly, the residue N84 and the neighbouring residues R128 and S218, equivalents to R62 and S151 of human WIPI3, respectively, and exposed at the exterior of the protein, have been reported to participate in an additional potential lipid binding site III (47). Positive charges around this region (Figure 6B) would govern the electrostatic interaction with other negatively charged partners such as phosphoinositide molecules. Moreover, the comparison of HsWIPI3 with the AtATG18a model reveals an increase of positive charge distribution on the surface of site III in the Arabidopsis protein (Supp. Fig. 9).

Consistent with this, persulfidation of C103 could potentially affect the molecular recognition in its neighboring protein region and consequently the function of AtATG18a. The cysteine persulfidation by the addition of –SH group to C103 could cause significant conformational changes due to: (1) a steric perturbation in the cavity (Figure 6C), destabilizing the original hydrophobic interactions and promoting new ones, and (2) an effect of negative charges from the deprotonation of -SSH group in a highly unipolar environment. The additional sulfur atom would contribute with a covalent radius of 1.02 Å, while that of hydrogen is 0.37 Å. It is worth mentioning that the aromatic-thiol π hydrogen bonding interaction is very sensitive to the orientation of the two lone electron pairs on the sulfur atom relative

to the π electron cloud of the phenyl ring (51). In addition, it would be reasonable to expect that persulfidation of C103 would introduce negative charges at the active site since -SSH group most probably would be completely deprotonated at physiological pH (22, 52). The replacement C103S could also destabilize the hydrophobic cavity site but in a different manner. Although the energetic cost of desolvating serine (-OH) is higher than for a cysteine (-SH) residue, the steric effect due its replacement would be much smaller than that caused by the additional –SH group (Figure 6B).Altogether, the C103 modification by persulfidation likely could cause a conformational change and intramolecular rearrangement of the cavity favouring the interaction with additional phosphoinositide molecules at site III and/or increasing the binding affinity of PtdIns(3)P for its target at site II through an allosteric cooperative effect.

Discussion

Autophagy regulation in plants has become an important, although challenging, topic in recent years, due to its involvement in plant health and cellular homeostasis, helping plants to tolerate different stresses such as oxidative stress, pathogen infection, nutrient deprivation, and drought (35, 36, 53, 54). It is now well known that ER stress triggers autophagy both in mammals and plants (37, 55), as a protective mechanism against misfolded proteins accumulating in the ER. Thus, a selective autophagy pathway named ER-phagy is activated to recycle accumulated misfolded proteins in the ER in order to restore ER homeostasis (56). In plants, it has been shown that inositol-requiring enzyme 1 (IRE1) is necessary for ER-phagy, and the delivery of ER to the vacuole for degradation under ER stress depends on the ATG18a protein (37). In mammals, recent studies showed that H_2S may influence ER stress, playing an important role in many heart, neurological, and respiratory diseases (57). In plants, H_2S sulfide was shown to negatively regulate bulk autophagy under nutrient deprivation, independently of redox conditions (28, 31). This mechanism was explained by persulfidation of ATG core proteins (16, 32). In this work, we have demonstrated that sulfide also regulates autophagy induced by ER stress, and this regulation was independent of its indirect antioxidant effect. Furthermore, we showed that sulfide played a signaling role in ER degradation by autophagy.

Although little has been reported about the biochemical function of plant ATG18a protein, in yeast and mammals a function for the Atg2-Atg18 complex in autophagy has been reported, and the binding of Atg18 to PtdIns(3)P is crucial in autophagy induction (58). Post-translational modifications of ATG18 are known to control its activity. Atg18 in the yeast *Pichia pastoris* was shown to be phosphorylated, and phosphorylation enhanced its binding affinity to PtdIns(3)P (59). However, this modification in *P. pastoris* does not affect autophagy activity, while phosphorylation of Arabidopsis ATG18a inhibits its function in autophagy (60). Therefore, posttranslational regulation of ATG18a must be finely controlled, and probably triggered depending on the stress to which the plant is subjected. Furthermore, ATG18a is also required for bulk autophagy and persulfidation could possibly regulate its activity in multiple stresses in addition to ER stress.

In this study, we explored the functional importance of sulfide in regulating ATG18a binding to PtdIns(3)P. Mass spectrometry analysis of recombinant ATG18a showed that only one Cys residue, C103, was persulfidated under our experimental conditions. Protein persulfidation at more than one Cys residue is rarely found in the literature, and the other Cys residues of ATG18a were not detected as modified peptides, indicating that C103 was the only target for persulfidation. Furthermore, this PTM was shown to be H_2S dose dependent at very low concentrations of NaHS and reversible by reducing agents, suggesting this modification may have a biological role in plants. We further showed the potential physiological role of the persulfidation of ATG18a by using WT and C103 mutant recombinant proteins in an *in vitro* assay; one important finding was that persulfidation of ATG18a increased its affinity for PtdIns(3)P, while impairment of persulfidation abolished almost completely this binding to phospholipids. In vivo, sulfide enhanced the fraction of ATG18a bound to membranes, while the mutant ATG18a_C103S was not affected by sulfide treatment and in general, the ATG18a_C103S fraction bound to membranes was less than that of the WT ATG18a protein.

We observed that the mutant protein ATG18a_C103S, impaired in persulfidation, was unable to bind properly to PtdIns(3)P, and therefore the colocalization time with an autophagosome marker was shorter than that of the wildtype protein. Furthermore, autophagosomes in plants expressing only the ATG18a_C103S mutated version had a smaller average size than when the WT counterpart was expressed. However, it seems that plants respond to this situation by increasing the number of

autophagosomes. ATG18a forms a complex with ATG2 that is involved in the expansion of the membrane of the autophagosome for phagophore elongation (61), therefore, it makes sense than disturbing the binding affinity of ATG18a for phosphoinositides could affect autophagosome size. In addition, the colocalization time of ATG18a_C103S with autophagosomes is shorter and its binding affinity to PtdIns(3)P is weaker than the WT ATG18a, resulting in an outcome of smaller autophagosomes, suggesting that C103 is important in regulating elongation of phagophore membranes. Previous studies in yeast demonstrated that insufficient levels of Atg7 affect both autophagosome size and number (62), and similarly, mutations disturbing Atg3 function also affect autophagosome size (63). The fact that misfunction of ATG18a has an effect on both autophagosome size (expansion) and number (nucleation) of autophagosomes may indicate that ATG18a could have additional roles in autophagosome formation.

In yeast, it was demonstrated that Atg18 is important for the localization of the Atg2-Atg18 complex to the pre-autophagosomal structure (PAS), through its PtdIns(3)P-binding ability (64, 65). In fact, some studies showed that autophagosome formation could efficiently progress in *atg2*Δ*atg18*Δ cells expressing engineered variants of Atg2 that are capable of localizing to the pre-autophagosomal structure (PAS). Engineered yeast expressing Atg2–HG–FYVE, a fusion of Atg2 with the phosphatidylinositol 3-phosphate-binding FYVE domain, or Atg2–HG–Atg8, expressing Atg2 fused with the core autophagy protein Atg8, allowed a partial recovery of autophagosome formation independently of Atg18 (66). Nevertheless, the partial recovery suggested that Atg18 possesses other functions beyond targeting Atg2 to the PAS. The general structure of this complex is similar to the mammalian homolog ATG2B-WIPI4, suggesting that the overall shape and function is evolutionarily conserved among species (67, 68). Our results obtained from the 3D structural alignment suggested that persulfidation of C103 could modulate the interaction with PtdIns(3)P molecules by inducing a conformational change of the surrounding site that could affect recognition of potential partners such as PtdIns(3)P through the electrostatic interaction network. Therefore, persulfidation of ATG18a could affect autophagy progression by regulating its PtdIns(3)P-binding affinity.

It is noteworthy that previous studies described how sulfide regulates bulk autophagy triggered by nutrient starvation or ABA (16, 31) and in this study, we demonstrate that ER-induced autophagy is also negatively regulated by sulfide. We provide a new level of regulation of autophagy in plant systems by sulfide, through the persulfidation of ATG18a. Together, our data suggest a model in which the dynamics of ATG18a association with forming autophagosomes is critical for autophagy during ER stress. The reversible persulfidation of ATG18a increases its binding to membranes via association with PtdIns(3)P, but potentially delays its release, inhibiting autophagosome maturation. Preventing persulfidation by mutation of C103 decreases its membrane affinity and localization time to phagophores. As ATG18a is thought to be involved in lipid transfer during autophagosome expansion, this decreased phagophore localization leads to the production of smaller autophagosomes. Autophagosome numbers increase, potentially to compensate for this. In this way, persulfidation of ATG18a may modulate the extent of autophagosome production during stress to ensure an appropriate physiological response.

Materials and methods

A detailed description of all materials and methodology is included in SI Appendix, Materials and Methods. This includes the expression and purification of recombinant Glutathione S-transferase (GST)-tagged protein, mass spectrometry, persulfide detection in cell lysates, plant genotypes, protein modelling, protein-lipid binding assay, membrane fractionation, autophagy detection, microscopy, bZIP60 splicing assay and expression and purification of free Glutathione S-transferase (GST) protein.

Data Availability.

All study data are included in the main text and SI Appendix.

Acknowledgments

This work was supported in part by the European Union's Horizon 2020 research and innovation programme under the Marie Skłodowska-Curie grant agreement No. 834120.

We also acknowledge I+D+I Project US-1255781 FEDER Andalucía 2014-2020 Operational Programme, for funding support (to A.A), Government of Aragón-FEDER grant E35_17R (to I. Y.), Agencia Estatal Investigación-ERDF grant PID2019-109785GB-I00 (to C.G.) and National Institutes of Health grant 1R01GM120316-01A1 (to D.C.B).
We thank Dr. F.J. Quintero and Dr. J.M. Pardo for providing anti-H^+ATPase antibody.

References

1. Bassham DC (2009) Function and regulation of macroautophagy in plants. *Biochimica et Biophysica Acta (BBA) - Molecular Cell Research* 1793(9):1397-1403.
2. Bassham D, *et al.* (2006) Autophagy in Development and Stress Responses of Plants. *Autophagy* 2:2-11.
3. Zientara-Rytter K & Sirko A (2016) To deliver or to degrade - an interplay of the ubiquitin-proteasome system, autophagy and vesicular transport in plants. *The FEBS journal* 283(19):3534-3555.
4. Pankiv S, *et al.* (2007) p62/SQSTM1 binds directly to Atg8/LC3 to facilitate degradation of ubiquitinated protein aggregates by autophagy. *J Biol Chem* 282(33):24131-24145.
5. Reggiori F, Komatsu M, Finley K, & Simonsen A (2012) Autophagy: more than a nonselective pathway. *International journal of cell biology* 2012:219625.
6. Kraft C, Reggiori F, & Peter M (2009) Selective types of autophagy in yeast. *Biochimica et Biophysica Acta (BBA) - Molecular Cell Research* 1793(9):1404-1412.
7. Liu Y, *et al.* (2012) Degradation of the Endoplasmic Reticulum by Autophagy during Endoplasmic Reticulum Stress in *Arabidopsis*. *The Plant cell* 24(11):4635-4651.
8. Wu J, *et al.* (2021) ATI1 (ATG8-interacting protein 1) and ATI2 define a plant starvation-induced reticulophagy pathway and serve as MSBP1/MAPR5 cargo receptors. *Autophagy*:1-14.
9. Johansen T & Lamark T (2011) Selective autophagy mediated by autophagic adapter proteins. *Autophagy* 7(3):279-296.
10. Lei Y & Klionsky DJ (2019) UIM-UDS: a new interface between ATG8 and its interactors. *Cell Research* 29(7):507-508.
11. Marshall RS, Hua Z, Mali S, McLoughlin F, & Vierstra RD (2019) ATG8-Binding UIM Proteins Define a New Class of Autophagy Adaptors and Receptors. *Cell* 177(3):766-781.e724.
12. Johansen T & Lamark T (2020) Selective Autophagy: ATG8 Family Proteins, LIR Motifs and Cargo Receptors. *Journal of Molecular Biology* 432(1):80-103.
13. Woo J, Park E, & Dinesh-Kumar SP (2014) Differential processing of Arabidopsis ubiquitin-like Atg8 autophagy proteins by Atg4 cysteine proteases. *Proc Natl Acad Sci U S A* 111(2):863-868.
14. Perez-Perez ME, Zaffagnini M, Marchand CH, Crespo JL, & Lemaire SD (2014) The yeast autophagy protease Atg4 is regulated by thioredoxin. *Autophagy* 10(11):1953-1964.
15. Perez-Perez ME, Lemaire SD, & Crespo JL (2016) Control of Autophagy in Chlamydomonas Is Mediated through Redox-Dependent Inactivation of the ATG4 Protease. *Plant Physiol.* 172(4):2219-2234.
16. Laureano-Marín AM, *et al.* (2020) Abscisic Acid-Triggered Persulfidation of the Cys Protease ATG4 Mediates Regulation of Autophagy by Sulfide. *The Plant cell* 32(12):3902-3920.

17. Pajares M, Cuadrado A, Engedal N, Jirsova Z, & Cahova M (2018) The Role of Free Radicals in Autophagy Regulation: Implications for Ageing. *Oxidative medicine and cellular longevity* 2018:2450748.
18. Scherz-Shouval R, *et al.* (2007) Reactive oxygen species are essential for autophagy and specifically regulate the activity of Atg4. *The EMBO journal* 26(7):1749-1760.
19. Pengo N, Agrotis A, Prak K, Jones J, & Ketteler R (2017) A reversible phospho-switch mediated by ULK1 regulates the activity of autophagy protease ATG4B. *Nature communications* 8(1):294.
20. Shivaraj SM, *et al.* (2020) Nitric oxide and hydrogen sulfide crosstalk during heavy metal stress in plants. *Physiologia plantarum* 168(2):437-455.
21. Xie Y, *et al.* (2015) Posttranslational modification of autophagy-related proteins in macroautophagy. *Autophagy* 11(1):28-45.
22. Filipovic MR, Zivanovic J, Alvarez B, & Banerjee R (2018) Chemical Biology of H2S Signaling through Persulfidation. *Chemical Reviews* 118(3):1253-1337.
23. Kimura H (2015) Physiological Roles of Hydrogen Sulfide and Polysulfides. *Handb. Exp. Pharmacol.* 230:61.
24. Aroca A, Gotor C, Bassham DC, & Romero LC (2020) Hydrogen Sulfide: From a Toxic Molecule to a Key Molecule of Cell Life. *Antioxidants* 9(7):621.
25. Aroca A, Serna A, Gotor C, & Romero L, C. (2015) S-sulfhydration: a cysteine posttranslational modification in plant systems. *Plant Physiology* 168(1):334-342
26. Aroca A, Schneider M, Scheibe R, Gotor C, & Romero LC (2017) Hydrogen Sulfide Regulates the Cytosolic/Nuclear Partitioning of Glyceraldehyde-3-Phosphate Dehydrogenase by Enhancing its Nuclear Localization. *Plant and Cell Physiology* 58(6):983-992.
27. Filipovic MR (2015) Persulfidation (S-sulfhydration) and H_2S. *Handbook of experimental pharmacology* 230:29-59.
28. Álvarez C, *et al.* (2012) Cysteine-generated sulfide in the cytosol negatively regulates autophagy and modulates the transcriptional profile in Arabidopsis. *The Plant cell* 24(11):4621-4634.
29. Zhang D, *et al.* (2014) Detection of Protein S-Sulfhydration by a Tag-Switch Technique. *Angewandte Chemie International Edition* 53(2):575-581.
30. Kundu S, Pushpakumar S, Khundmiri SJ, & Sen U (2014) Hydrogen sulfide mitigates hyperglycemic remodeling via liver kinase B1-adenosine monophosphate-activated protein kinase signaling. *Biochimica et biophysica acta* 1843(12):2816-2826.
31. Laureano-Marin AM, Moreno I, Romero LC, & Gotor C (2016) Negative Regulation of Autophagy by Sulfide Is Independent of Reactive Oxygen Species. *Plant Physiol* 171(2):1378-1391.
32. Aroca A, Benito JM, Gotor C, & Romero LC (2017) Persulfidation proteome reveals the regulation of protein function by hydrogen sulfide in diverse biological processes in Arabidopsis. *Journal of experimental botany* 68(17):4915-4927.
33. Dove SK, *et al.* (2004) Svp1p defines a family of phosphatidylinositol 3,5-bisphosphate effectors. *The EMBO journal* 23(9):1922-1933.
34. Wun C-L, Quan Y, & Zhuang X (2020) Recent Advances in Membrane Shaping for Plant Autophagosome Biogenesis. *Frontiers in plant science* 11:565-565.
35. Liu Y, Xiong Y, & Bassham DC (2009) Autophagy is required for tolerance of drought and salt stress in plants. *Autophagy* 5(7):954-963.
36. Xiong Y, Contento AL, & Bassham DC (2005) AtATG18a is required for the formation of autophagosomes during nutrient stress and senescence in Arabidopsis thaliana. *The Plant journal : for cell and molecular biology* 42(4):535-546.

37. Liu Y, *et al.* (2012) Degradation of the Endoplasmic Reticulum by Autophagy during Endoplasmic Reticulum Stress in Arabidopsis. *The Plant cell* 24.
38. Zivanovic J, *et al.* (2019) Selective Persulfide Detection Reveals Evolutionarily Conserved Antiaging Effects of S-Sulfhydration. *Cell metabolism* 30(6):1152-1170.e1113.
39. Bernal-Perez LF, Prokai L, & Ryu Y (2012) Selective N-terminal fluorescent labeling of proteins using 4-chloro-7-nitrobenzofurazan: a method to distinguish protein N-terminal acetylation. *Analytical biochemistry* 428(1):13-15.
40. Malhotra J, *et al.* (2008) Antioxidants reduce endoplasmic reticulum stress and improve protein secretion. *Proceedings of the National Academy of Sciences of the United States of America* 105:18525-18530.
41. Aroca A, Gotor C, & Romero LC (2018) Hydrogen Sulfide Signaling in Plants: Emerging Roles of Protein Persulfidation. *Frontiers in plant science* 9(1369).
42. Xie Z-Z, Liu Y, & Bian J-S (2016) Hydrogen Sulfide and Cellular Redox Homeostasis. *Oxidative medicine and cellular longevity* 2016:6043038.
43. Batoko H, Zheng HQ, Hawes C, & Moore I (2000) A rab1 GTPase is required for transport between the endoplasmic reticulum and golgi apparatus and for normal golgi movement in plants. *The Plant cell* 12(11):2201-2218.
44. Deng Y, *et al.* (2011) Heat induces the splicing by IRE1 of a mRNA encoding a transcription factor involved in the unfolded protein response in Arabidopsis. *Proceedings of the National Academy of Sciences of the United States of America* 108(17):7247-7252.
45. Bakula D, *et al.* (2017) WIPI3 and WIPI4 β-propellers are scaffolds for LKB1-AMPK-TSC signalling circuits in the control of autophagy. *Nature communications* 8:15637-15637.
46. Baskaran S, Ragusa Michael J, Boura E, & Hurley James H (2012) Two-Site Recognition of Phosphatidylinositol 3-Phosphate by PROPPINs in Autophagy. *Molecular cell* 47(3):339-348.
47. Liang R, Ren J, Zhang Y, & Feng W (2019) Structural Conservation of the Two Phosphoinositide-Binding Sites in WIPI Proteins. *Journal of Molecular Biology* 431(7):1494-1505.
48. Humphry NJ & Wheatley SP (2018) Survivin inhibits excessive autophagy in cancer cells but does so independently of its interaction with LC3. *Biol Open* 7(10):bio037374.
49. Ren J, *et al.* (2020) Multi-site-mediated entwining of the linear WIR-motif around WIPI β-propellers for autophagy. *Nature communications* 11(1):2702.
50. Bakula D, *et al.* (2017) WIPI3 and WIPI4 β-propellers are scaffolds for LKB1-AMPK-TSC signalling circuits in the control of autophagy. *Nature communications* 8(1):15637.
51. Duan G, Smith VH, & Weaver DF (2001) Characterization of aromatic-thiol π-type hydrogen bonding and phenylalanine-cysteine side chain interactions through ab initio calculations and protein database analyses. *Molecular Physics* 99(19):1689-1699.
52. Cuevasanta E, *et al.* (2015) Reaction of Hydrogen Sulfide with Disulfide and Sulfenic Acid to Form the Strongly Nucleophilic Persulfide. *Journal of Biological Chemistry* 290(45):26866-26880.
53. Hanaoka H, *et al.* (2002) Leaf senescence and starvation-induced chlorosis are accelerated by the disruption of an Arabidopsis autophagy gene. *Plant Physiol* 129(3):1181-1193.

54. Signorelli S, Tarkowski ŁP, Van den Ende W, & Bassham DC (2019) Linking Autophagy to Abiotic and Biotic Stress Responses. *Trends in Plant Science* 24(5):413-430.
55. Lee WS, Yoo WH, & Chae HJ (2015) ER Stress and Autophagy. *Current molecular medicine* 15(8):735-745.
56. Grumati P, Dikic I, & Stolz A (2018) ER-phagy at a glance. *J Cell Sci* 131(17).
57. Wang H, Shi X, Qiu M, Lv S, & Liu H (2020) Hydrogen Sulfide Plays an Important Protective Role through Influencing Endoplasmic Reticulum Stress in Diseases. *Int J Biol Sci* 16(2):264-271.
58. Krick R, Tolstrup J, Appelles A, Henke S, & Thumm M (2006) The relevance of the phosphatidylinositolphosphat-binding motif FRRGT of Atg18 and Atg21 for the Cvt pathway and autophagy. *FEBS Letters* 580(19):4632-4638.
59. Tamura N, *et al.* (2013) Atg18 phosphoregulation controls organellar dynamics by modulating its phosphoinositide-binding activity. *The Journal of Cell Biology* 202(4):685-698.
60. Zhang B, *et al.* (2020) Phosphorylation of ATG18a by BAK1 Suppresses Autophagy and Attenuates Plant Resistance against Necrotrophic Pathogens. *Autophagy*.
61. Kang S, Shin KD, Kim JH, & Chung T (2018) Autophagy-related (ATG) 11, ATG9 and the phosphatidylinositol 3-kinase control ATG2-mediated formation of autophagosomes in Arabidopsis. *Plant cell reports* 37(4):653-664.
62. Cawthon H, Chakraborty R, Roberts JR, & Backues SK (2018) Control of autophagosome size and number by Atg7. *Biochemical and biophysical research communications* 503(2):651-656.
63. Sakoh-Nakatogawa M, Kirisako H, Nakatogawa H, & Ohsumi Y (2015) Localization of Atg3 to autophagy-related membranes and its enhancement by the Atg8-family interacting motif to promote expansion of the membranes. *FEBS Letters* 589(6):744-749.
64. Kotani T, Kirisako H, Koizumi M, Ohsumi Y, & Nakatogawa H (2018) The Atg2-Atg18 complex tethers pre-autophagosomal membranes to the endoplasmic reticulum for autophagosome formation. *Proceedings of the National Academy of Sciences of the United States of America* 115(41):10363-10368.
65. Obara K, Sekito T, Niimi K, & Ohsumi Y (2008) The Atg18-Atg2 complex is recruited to autophagic membranes via phosphatidylinositol 3-phosphate and exerts an essential function. *The Journal of biological chemistry* 283(35):23972-23980.
66. Kobayashi T, Suzuki K, & Ohsumi Y (2012) Autophagosome formation can be achieved in the absence of Atg18 by expressing engineered PAS-targeted Atg2. *FEBS Letters* 586(16):2473-2478.
67. Zheng JX, *et al.* (2017) Architecture of the ATG2B-WDR45 complex and an aromatic Y/HF motif crucial for complex formation. *Autophagy* 13(11):1870-1883.
68. Chowdhury S, *et al.* (2018) Insights into autophagosome biogenesis from structural and biochemical analyses of the ATG2A-WIPI4 complex. *Proceedings of the National Academy of Sciences of the United States of America* 115(42):E9792-e9801.

Figure Legends

Figure 1. Mass spectrometry analysis of AtATG18a and in-gel detection of recombinant AtATG18a protein persulfide labeling (A) The protein was identified with a sequence coverage of 79% highlighted in blue; Cysteines are highlighted in yellow and the peptide containing persulfidated Cys-103 is shown in red underlined. (B) LC-MS/MS analysis of the tryptic peptide containing Cys-103 of ATG18a. The table inside the spectrum contains the predicted ion types for the modified peptide,

and the ions detected in the spectrum are highlighted in red and blue. (C) Scheme of dimedone-switch method used to label persulfides with DAz-2/Cy5-alkyne. (D-E) In-gel detection of recombinant AtATG18a protein persulfide labeling which is represented in fire pseudo-coloring to visually enhance the signal. Green fluorescence corresponds to the total protein loaded (NBF-protein adducts). Increasing concentrations of the sulfide donors NaHS (D) and Na_2S_4 (E) were used and two reducing agents, 5mM TCEP or 25mM DTT. Control samples were untreated (labeled as C). Ratio of Cy5/NBF signals is used for the quantification represented in the graphs. Data is shown as the mean ± SD of 3 individual experiments. *p < 0.01 versus control.

Figure 2. **ER-stress induced autophagy is regulated by sulfide in *Arabidopsis* roots.** Seven-day-old GFP-ATG8e transgenic plants were transferred to MS liquid medium supplemented with TM to induce ER stress, sulfide (NaHS), ascorbic acid (ASC) and/or glutathione (GSH), or DMSO (Control) (A) GFP-ATG8e–labeled autophagosomes in root epidermal cells were visualized by confocal microscopy. Arrows indicate GFP-labeled autophagosomes or autophagic bodies. Insets show enlargement. Scale bars, 40 µm for main figure and 20 µm for insets. (B) Quantification of autophagosomes per frame for each treatment. Values are the mean ± SD. (n>15) Different letters indicate statistically significant differences (ANOVA, Fisher's least significant difference (LSD) test, $p < 0.05$). (C) Immunoblot analysis using anti-ATG8 antibodies in protein extracts from WT Arabidopsis seedlings treated with TM for 6, 12 and 24 hours and NaHS. Graph shows the relative band intensity. Bars represent means ± SD (n = 3).*p<0.01, ** $p < 0.05$.

Figure 3. ER degradation by autophagy is regulated by sulfide in *Arabidopsis* roots. Seven-day-old GFP-HDEL transgenic plants were transferred to MS liquid medium supplemented with tunicamycin (TM) for 6 h to induce ER stress, and sulfide (NaHS) for 1 h. DMSO was used as solvent (Control). ER structure in root epidermal cells was visualized by confocal microscopy, representative of 3-4 pictures/plant and 4-5 plants/treatment. Scale bars, 40 µm.

Figure 4. **Sulfide enhances ATG18a binding to membranes** (A) Schematic representation of the indicated membrane lipids on a PIP strip. Red dots represent the specific lipids PtdIns(3)P and PtdIns(3,5)P_2 for panels B and D. (B) Binding of recombinant GST-ATG18a proteins to PIP strips. 0.5 µg of protein was incubated with increasing concentration of NaHS and TCEP, followed by incubation with PIP strips. Bound protein was detected using anti-GST primary antibody and anti-rabbit-HRP secondary antibody. (C) Spot intensity relative quantification of panel B. (D) Comparison of binding affinity to PIP strips of 1 µg of GST-ATG18a and GST-ATG18a_C103S treated or not with 10 µM Na_2S_4. (E) Spot intensity relative quantification of panel D. (F) Immunoblot of soluble (SF) and membrane-bound (MB) fractions of the fusion proteins YFP-ATG18a and YFP-ATG18a_C103S, obtained from transgenic lines treated with tunicamycin (TM) for 6 hours and sulfide (NaHS) for 1 hour. (G) Relative band intensity quantification. In panels C, E and G, bars represent means ± SD (n = 3). Different letters indicate statistically significant differences (ANOVA, Turkey test, $p < 0.05$).

Figure 5. Time-lapse confocal fluorescence microscopy of autophagosomes in roots from 1-week-old seedlings treated with tunicamycin (TM) and sulfide (NaHS). (A) Confocal images for colocalization of YFP-ATG18a and YFP-ATG18a_C103S with Cer-ATG8e. Scale bars, 2 µm. (B) Analysis of YFP/Cerulean colocalization time. Duration of colocalization is represented in seconds. (n >15). (C) Confocal images for Cer-ATG8e in the double transgenic plants YFP-ATG18a/Cer-ATG8e and YFP-ATG18a_C103S/Cer-ATG8e after treatment with TM and NaHS. (D) Autophagosome size analysis measured with ImageJ, n = 150 (E) Autophagosome number quantification counted manually with ImageJ, n = 15. Values are the mean ± SD. Different letters indicate statistically significant differences (ANOVA, Fisher's least significant difference (LSD) test, $p< 0.05$).

Figure 6. Predicted structure of AtATG18. (A) Crystal structure of human WIPI3 (PDB ID: 6KRL, left panel) and predicted structural model of Arabidopsis ATG18a (right panel). The proposed lipid binding-sites and the cavity site of C103 are highlighted. The inset shows the residues of AtATG18a surrounding the active C103 site (F83, N84, D86 and F90) and participating in binding-site III (R128 and S218). The equivalent residues in HsWIPI3 are in grey. (B) Representation of surface electrostatic potential distribution in AtATG18a structural model and zoomed into the putative conformation of the active site, showing with spheres the position of C103, the persulfidation C103-SH, and the mutation C103S. Positively and negatively charged regions are depicted in blue and red, respectively. (C) Zoom into the putative conformation of the active site showing distance (Å) between the catalytic residue C103 and F83 and F90 in AtATG18a.

672

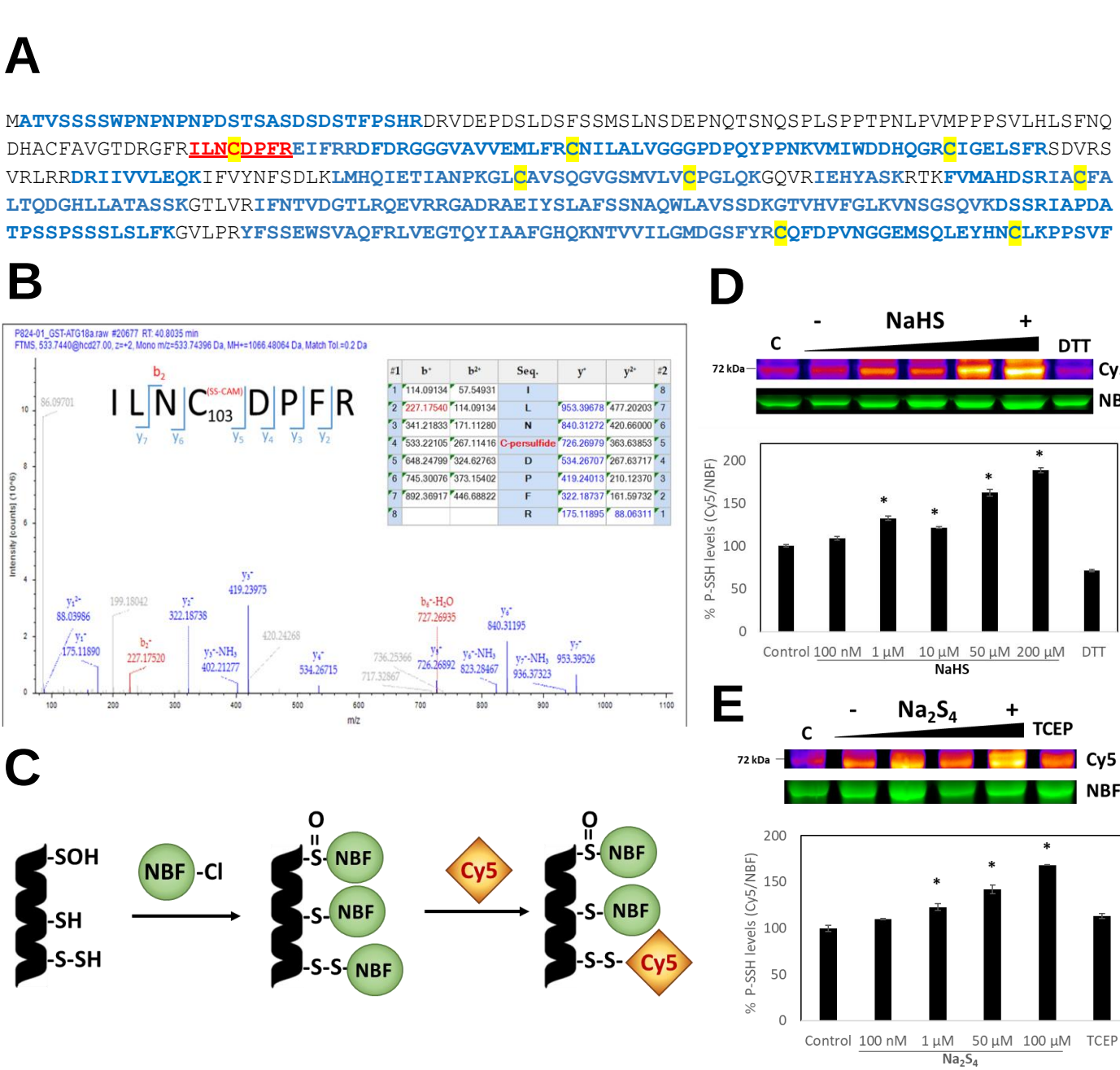

Figure 1. Mass spectrometry analysis of AtATG18a and in-gel detection of recombinant AtATG18a protein persulfide labeling (A) The protein was identified with a sequence coverage of 79% highlighted in blue; Cysteines are highlighted in yellow and the peptide containing persulfidated Cys-103 is shown in red underlined. (B) LC-MS/MS analysis of the tryptic peptide containing Cys-103 of ATG18a. The table inside the spectrum contains the predicted ion types for the modified peptide, and the ions detected in the spectrum are highlighted in red and blue. (C) Scheme of dimedone-switch method used to label persulfides with DAz-2/Cy5-alkyne. (D-E) In-gel detection of recombinant AtATG18a protein persulfide labeling which is represented in fire pseudo-coloring to visually enhance the signal. Green fluorescence corresponds to the total protein loaded (NBF-protein adducts). Increasing concentrations of the sulfide donors NaHS (D) and Na2S4 (E) were used and two reducing agents, 5mM TCEP or 25mM DTT. Control samples were untreated (labeled as C). Ratio of Cy5/NBF signals is used for the quantification represented in the graphs. Data is shown as the mean ± SD of 3 individual experiments. *p < 0.01 versus control.

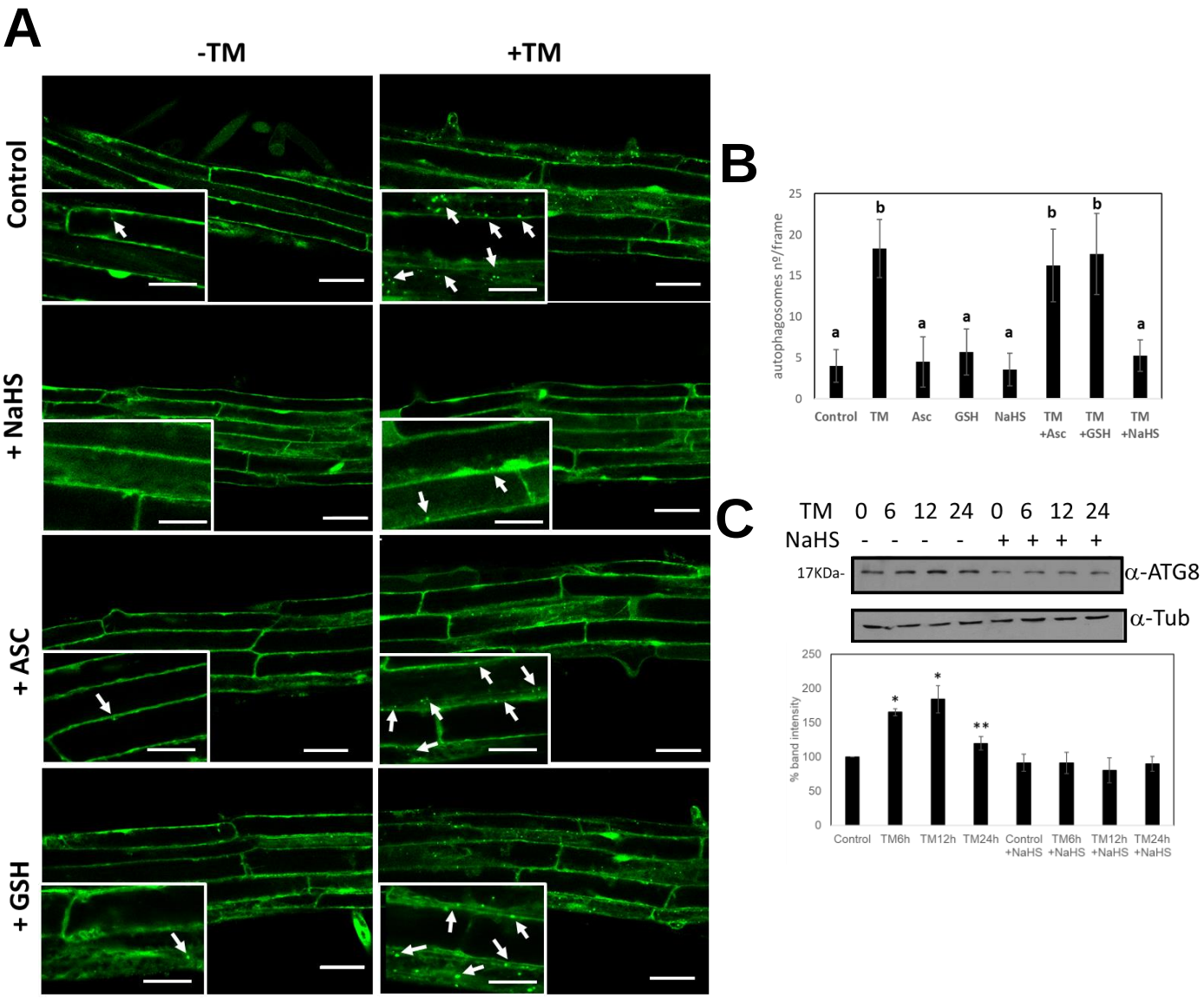

Figure 2. ER-stress induced autophagy is regulated by sulfide in Arabidopsis roots. Seven-day-old GFP-ATG8e transgenic plants were transferred to MS liquid medium supplemented with TM to induce ER stress, sulfide (NaHS), ascorbic acid (ASC) and/or glutathione (GSH), or DMSO (Control) (A) GFP-ATG8e–labeled autophagosomes in root epidermal cells were visualized by confocal microscopy. Arrows indicate GFP-labeled autophagosomes or autophagic bodies. Insets show enlargement. Scale bars, 40 μm for main figure and 20 μm for insets. (B) Quantification of autophagosomes per frame for each treatment. Values are the mean ± SD. (n>15) Different letters indicate statistically significant differences (ANOVA, Fisher's least significant difference (LSD) test, $p < 0.05$). (C) Immunoblot analysis using anti-ATG8 antibodies in protein extracts from WT Arabidopsis seedlings treated with TM for 6, 12 and 24 hours and NaHS. Graph shows the relative band intensity. Bars represent means ± SD (n = 3).*$p<0.01$, ** $p < 0.05$.

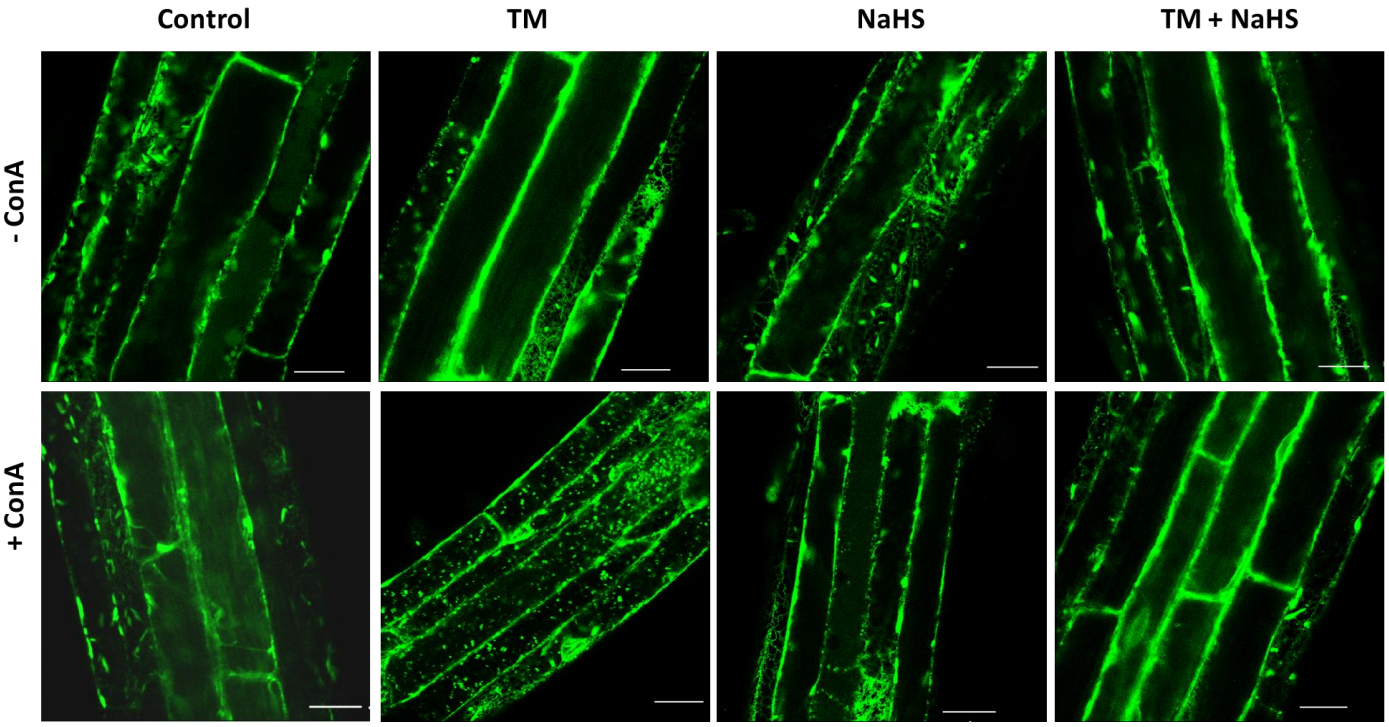

Figure 3. ER degradation by autophagy is regulated by sulfide in Arabidopsis roots. Seven-day-old GFP-HDEL transgenic plants were transferred to MS liquid medium supplemented with tunicamycin (TM) for 6 h to induce ER stress, and sulfide (NaHS) for 1 h. DMSO was used as solvent (Control). ER structure in root epidermal cells was visualized by confocal microscopy, representative of 3-4 pictures/plant and 4-5 plants/treatment. Scale bars, 40 μm.

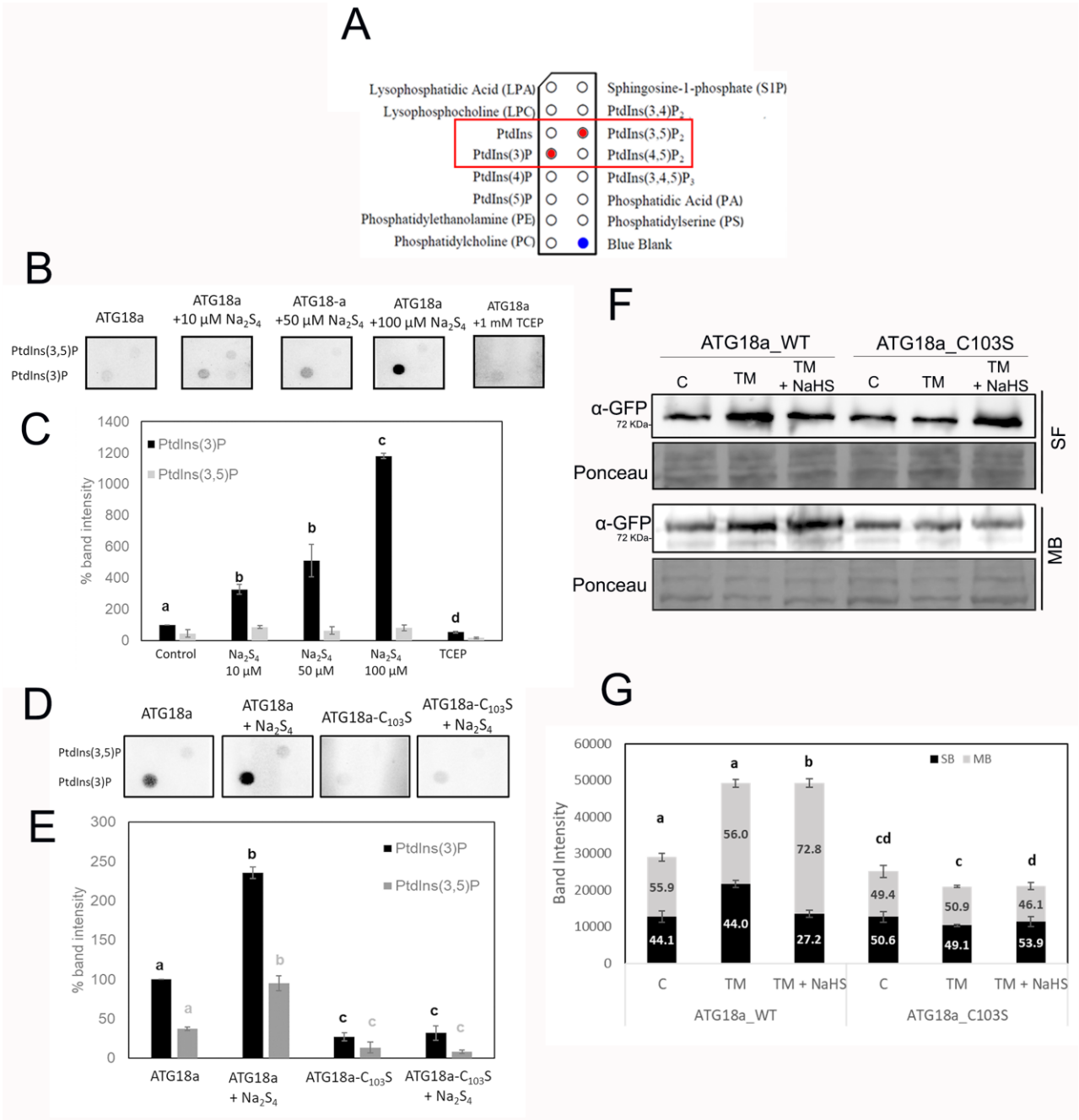

Figure 4. Sulfide enhances ATG18a binding to membranes (A) Schematic representation of the indicated membrane lipids on a PIP strip. Red dots represent the specific lipids PtdIns(3)P and PtdIns(3,5)P2 for panels B and D. (B) Binding of recombinant GST-ATG18a proteins to PIP strips. 0.5 µg of protein was incubated with increasing concentration of NaHS and TCEP, followed by incubation with PIP strips. Bound protein was detected using anti-GST primary antibody and anti-rabbit-HRP secondary antibody. (C) Spot intensity relative quantification of panel B. (D) Comparison of binding affinity to PIP strips of 1 µg of GST-ATG18a and GST-ATG18a_C103S treated or not with 10 µM Na2S4. (E) Spot intensity relative quantification of panel D. (F) Immunoblot of soluble (SF) and membrane-bound (MB) fractions of the fusion proteins YFP-ATG18a and YFP-ATG18a_C103S, obtained from transgenic lines treated with tunicamycin (TM) for 6 hours and sulfide (NaHS) for 1 hour. (G) Relative band intensity quantification. In panels C, E and G, bars represent means ± SD (n = 3). Different letters indicate statistically significant differences (ANOVA, Turkey test, $p < 0.05$).

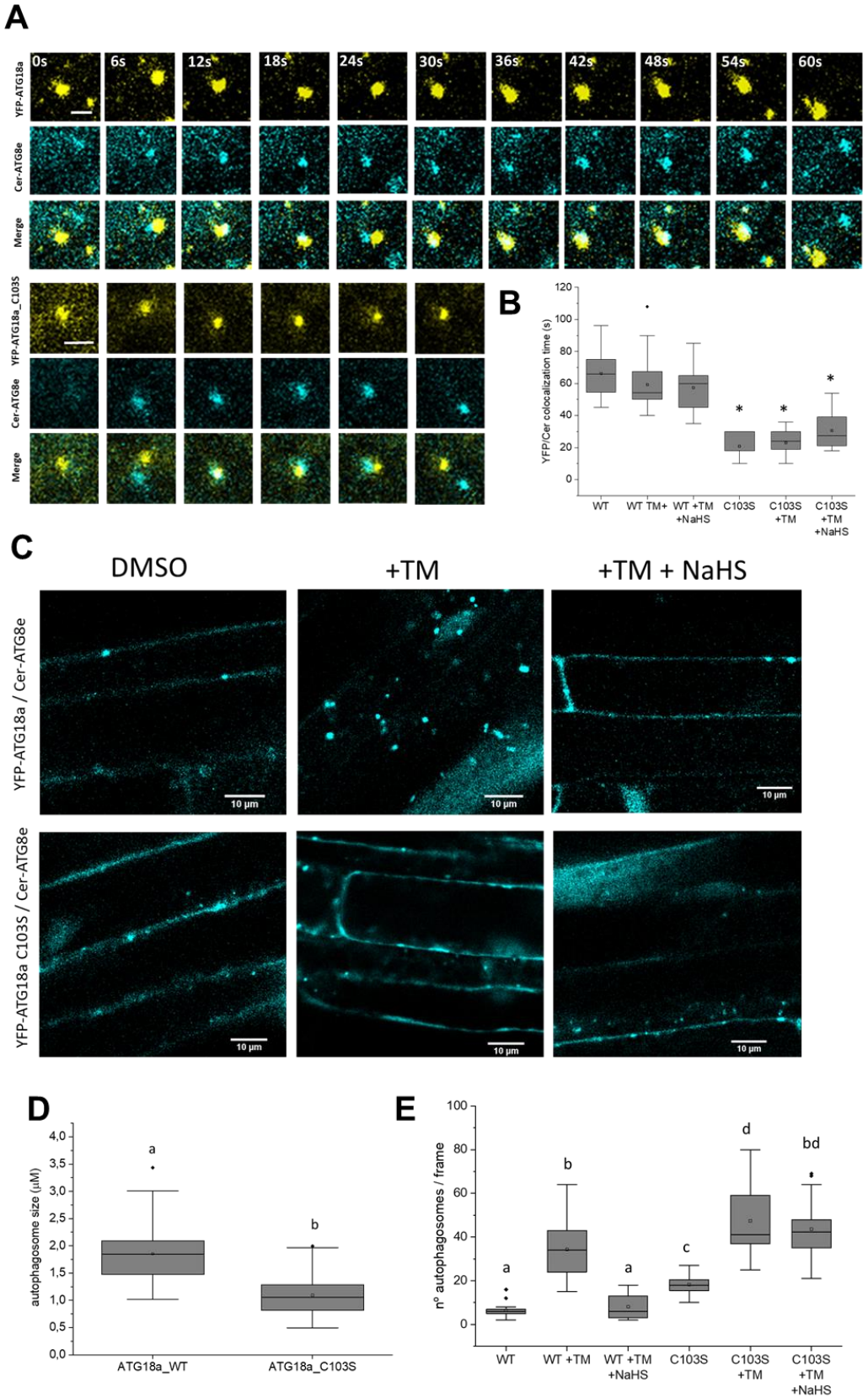

Figure 5. Time-lapse confocal fluorescence microscopy of autophagosomes in roots from 1-week-old seedlings treated with tunicamycin (TM) and sulfide (NaHS). (A) Confocal images for colocalization of YFP-ATG18a and YFP-ATG18a_C103S with Cer-ATG8e. Scale bars, 2 µm. (B) Analysis of YFP/Cerulean colocalization time. Duration of colocalization is represented in seconds. (n >15). (C) Confocal images for Cer-ATG8e in the double transgenic plants YFP-ATG18a/Cer-ATG8e and YFP-ATG18a_C103S/Cer-ATG8e after treatment with TM and NaHS. (D) Autophagosome size analysis measured with ImageJ, n = 150 (E) Autophagosome number quantification counted manually with ImageJ, n = 15. Values are the mean ± SD. Different letters indicate statistically significant differences (ANOVA, Fisher's least significant difference (LSD) test, $p < 0.05$)

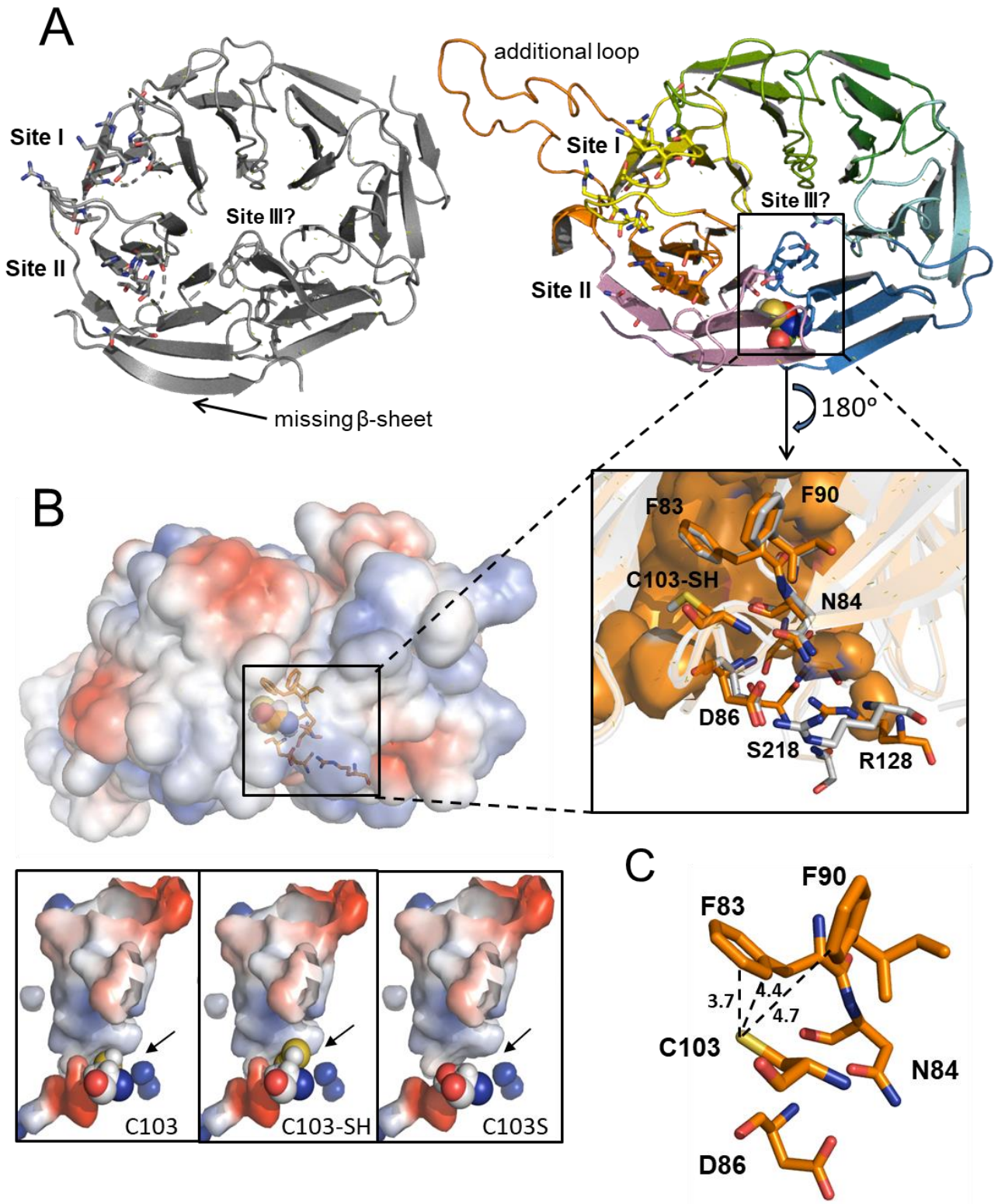

Figure 6.- Predicted structure of AtATG18. (A) Crystal structure of human WIPI3 (PDB ID: 6KRL, left panel) and predicted structural model of Arabidopsis ATG18a (right panel). The proposed lipid binding-sites and the cavity site of C103 are highlighted. The inset shows the residues of AtATG18a surrounding the active C103 site (F83, N84, D86 and F90) and participating in binding-site III (R128 and S218). The equivalent residues in HsWIPI3 are in grey. (B) Representation of surface electrostatic potential distribution in AtATG18a structural model and zoomed into the putative conformation of the active site, showing with spheres the position of C103, the persulfidation C103-SH, and the mutation C103S. Positively and negatively charged regions are depicted in blue and red, respectively. (C) Zoom into the putative conformation of the active site showing distance (Å) between the catalytic residue C103 and F83 and F90 in AtATG18a.

PNAS
www.pnas.org

Supplementary Information for

Persulfidation of ATG18a regulates autophagy under ER stress in Arabidopsis.

Angeles Aroca [1,2 *], Inmaculada Yruela [3,4], Cecilia Gotor [2], Diane C. Bassham[1]

*Angeles Aroca
Email: aroca@us.es

This PDF file includes:

Supplementary text
Figures S1 to S9
Tables S1 to S1
SI References

Supplementary Information Text

Material and methods

*Expression and Purification of Recombinant Glutathione S-transferase (*GST*)-Tagged Protein*

The complete complementary DNA of AtATG18a (At3g62770) was cloned into the pDEST15 vector using Gateway Technology (Invitrogen) to express an N-terminal GST-tagged protein using the *Escherichia coli* expression system. Primers C103S (F/R) (Suppl. Table 1) were used to mutate the pDEST15-ATG18a construct to generate pDEST15-ATG18a_C103S.

For protein expression, transformed E. coli BL21 (DE3) cell cultures at an optical density at 600 nm of 0.6 were treated with 0.5 mM isopropyl-β-D-thiogalactopyranoside and incubated for 4 h at 30°C. Purification was performed by GST resin binding under non-denaturing conditions using the GST-Bind Kit (Novagen) according to the manufacturer's recommendations. Recombinant protein production and purification was assessed by SDS-PAGE using 10% (w/v) polyacrylamide gels and Coomassie Brilliant Blue staining.

Mass Spectrometry

A total of 180 µg of purified recombinant GST-ATG18a, *in vivo* persulfidated by *E.coli*, was analyzed by LC-MS/MS. The protein Cys residues were modified with iodoacetamide, without the reduction step, and trypsin-digested. Formic acid was added to stop digestion before drying down the samples in a SpeedVac. Samples were desalted using C18 MicroSpin Columns (Nest Group SEM SS18V) before drying again in a SpeedVac. The peptides were then separated by liquid chromatography in a Thermo Scientific EASY nLC-1200 coupled to a Thermo Scientific Nanospray FlexIon source, using a pulled glass emitter 75um X 20 cm (Agilent capillary). The tip is packed with C18 packing material (Agilent Zorbax Chromatography Packing, SB-C18, 5 micron) and the remainder of the column is packed with UChrom 3 micron material from nanoLCMS Solutions. Peptides were separated using a 120-min gradient using buffer A: 0.1% formic acid/water and buffer B: 0.1% formic acid/acetonitrile. Data acquisition was performed with a Thermo Scientific Q Exactive Hybrid Quadrupole-Orbitrap Mass Spectrometer with an HCD fragmentation cell. The resulting intact and fragmentation pattern is compared to a theoretical fragmentation pattern (from Sequest HT) to find peptides that can be used to identify the proteins. MS survey scans in the mass range of 350–5000 Da were performed. Two biological replicates and two technical replicates were analysed.

MS and MS/MS data obtained were processed using Thermo Scientific's Proteome Discoverer Software. Searches were done with an *Arabidopsis thaliana* protein database from UniProt. Search parameters were set as follows: Oxidation / +15.995 Da (M); Deamidated / +0.984 Da (N, Q); Carbamidomethyl / +57.021 Da (C); Sulfide / +31.972 Da (C) as dynamic modifications. The peptide mass tolerance was set to 10 ppm and 0.02 Da for fragment masses, and 2 missed cleavages were allowed. False discovery rates (FDR ≤ 1% at the PSM level) for peptide identification were manually calculated.

Persulfide detection in cell lysates

A total of 1 mg of purified recombinant GST-ATG18a in PBS supplemented with 1% protease inhibitor (cOmplete™, SigmaAldrich) was incubated with increasing NaHS and Na_2S_4 concentrations from 100 nM to 200 µM, and 5mM TCEP or 25mM DTT as described in Figure 2. Then, samples were incubated with 5 mM 4-chloro-7-nitrobenzofurazan (Cl-NBF) at 37 ºC for 30 min, protected from light. A methanol/chloroform precipitation was performed to eliminate excess Cl-NBF and protein pellets obtained were washed with cold methanol, dried and re-dissolved in 50 mM PBS with 2% SDS. Proteins were then incubated with 25 µM DAz-2:Cy-5 pre-click mix at 37 ºC for 30 min (1 mM DAz-2 (Cayman chemical), 1 mM Cyanine5 alkyne (lumiprobe), 2 mM

copper(II)-TBTA complex (Lumiprobe), 4 mM ascorbic acid, 15 mM PBS and 30% acetonitrile, mixed overnight at RT and quenched with 20 mM EDTA). Following incubation, methanol/chloroform precipitation was performed and pellets washed with methanol as described above. The protein labelling was analysed by SDS-PAGE. After SDS-PAGE, gels were fixed for 30 min in 12.5% methanol and 4% acetic acid, protected from light. The gel was imaged at 640 nm for Cy5 signal and 488 nm for NBF-Cl signal on a Typhoon FLA 9500 (GE healthcare).

Plant genotypes

All lines used in this study were in the Columbia-0 (Col-0) background.

Transgenic plants expressing green fluorescent protein (GFP)-ATG8e (1) and GFP-HDEL (His-Asp-Glu-Leu peptide) (2) have been previously described. The complete complementary DNA of AtATG18a (At3g62770) was cloned into the binary plasmid pUBQ10:YFP-GW, obtained from the Arabidopsis Biological Resource Center (ABRC), to produce the construct pUBQ10:YFP-ATG18a. The plasmid pPZP211-35S:Cerulean-ATG8 as previously described was used to transform Arabidopsis plants (3). Homozygous *atg18a* T-DNA insertion mutant (GABI_651D08) seeds were kindly provided by Dr. Sanchez-Coll (4). Primers C103S (F/R) (Suppl. Table 1) were used to mutate C103 of ATG18a into Serine in the plasmid pUBQ10:YFP-ATG18a to produce the construct pUBQ10:YFP-ATG18a_C103S. Primers used in this work are described in Supplemental Table 1. The constructs described above were introduced into *Agrobacterium tumefaciens* strain GV3101 by heat shock. Δ*atg18a* T-DNA insertion mutant Arabidopsis plants were co-transformed by the floral dip method (5), using the pUBQ10:YFP-ATG18a or pUBQ10:YFP- ATG18a-C103S, and pPZP211-35S:Cerulean-ATG8. For cotransformation, Agrobacterium suspensions were mixed equally before dipping. Transformants were selected using the relevant antibiotic markers and confirmed by fluorescence microscopy.

Seeds were sterilized in 33% (v:v) bleach with 0.1% (v:v) Triton X-100 (Fisher Scientific, BP151) for 20 min, followed by washing with sterile water at least 5 times. After being stratified in the dark at 4°C for at least 48 h, sterilized seeds were plated and germinated on ½ strength MS solid medium (Murashige & Skoog vitamin and salt mixture [Caisson Laboratories, MSP01], 0.5% [w:v] sucrose [SigmaAldrich, S0389], 2.4 mM MES [Sigma-Aldrich, M3671], pH 5.7, and 0.6% [w:v] phytoagar [Caisson Laboratories, PTP01]). Unless otherwise noted, plants were grown at 22°C in long day conditions (16 h light/8 h dark).

Protein modelling

3D homology modelling and structural alignment was driven with HHPred (https://toolkit.tuebingen.mpg.de/tools/hhpred) and Modeller (6) using the structure of the *Homo sapiens* WIPI3 - ATG2A:WIR-peptide complex (PDB ID: 6KLR; (7)) as template. 3D alignment of a structural model of *Arabidopsis thaliana* AtATG18a and molecular crystal X-ray structure was performed with PyMol 1.4.1 (Schrodinger LLC).

Protein-lipid binding assay

PIP (phosphatidylinositol) strips (Echelon Biosciences) were blocked with 1% fatty acid-free milk in TBS / 0.1% Tween20 for 1h at RT, and incubated for 1 more h with 0.5 µg of purified recombinant GST-ATG18a, GST-ATG18a_C103S, or free GST as control. Purified proteins were treated with increasing concentrations of Na_2S_4 (10-100 µM) or 1 mM TCEP prior to incubation with the PIP strips. The membranes were then washed four times in TBS buffer. After washing, membranes were incubated with polyclonal anti-GST (Novus Biologicals) at 1:10,000 dilution for 1 hr at 4 °C, followed by additional washing and incubation with goat anti-rabbit-IgG-horseradish peroxidase-

conjugated antibody at 1:20,000. After final washing, membrane-bound GST-ATG18a was visualized by chemi-luminescence.

Membrane fractionation

For membrane fractionation, 1 week-old pUBQ10:YFP-ATG18a and pUBQ10:YFP- ATG18a-C103S Arabidopsis seedlings on MS medium were placed in liquid MS medium supplemented with 5µg/ml Tunicamycin (TM) for 6 hours and incubated or not for 1h with 200 µM NaHS. For total protein extraction, seedlings were ground in liquid nitrogen and homogenized in ice-cold protein extraction buffer (50 mM TRIS pH 7.5, 150mM NaCl) supplemented with protease inhibitor cocktail (cOmplete™, SigmaAldrich). The samples were then centrifuged at 4°C at 100,000*g* for 30 min. The supernatant was considered the soluble fraction and pellet was homogenized in 50 mM TRIS pH 7.5, 150mM NaCl and considered as the membrane bound fraction. Fractions were separated by SDS-PAGE, and transferred to a nitrocellulose membrane (GE Healthcare Amersham) to be analysed using anti-GFP (1:3000; Invitrogen), anti-OASA1 (1:10000) (8) and anti-H^+ATPase (1:10000)(9).

Autophagy detection

For autophagy analysis, 1 week-old GFP-ATG8e, pUBQ:GFP-ATG8 and GFP-HDEL Arabidopsis seedlings on MS medium were placed in liquid MS medium supplemented with 5µg/ml Tunicamycin (TM) for specified time, (6, 12 or 24 hours (or GFP-ATG8e, pUBQ:GFP-ATG8 genotypes, and only 6 hours for GFP-HDEL plants) and incubated or not for 1h with 200 µM NaHS. Control treatment was performed with DMSO. For autophagy detection under nitrogen starvation assay, 1 week-old YFP-ATG18a/Cerulean-ATG8 and YFP- ATG18a-C103S/Cerulean-ATG8 Arabidopsis seedlings were transferred to nitrogen-deficient MS medium for 4 days, supplemented or not with 200 µM NaHS. For total protein extraction, seedlings were ground in liquid nitrogen and homogenized in ice-cold protein extraction buffer (50 mM TRIS at pH 7.5, 150mM NaCl) supplemented with protease inhibitor cocktail (Roche). The samples were then centrifuged at 4°C at 8,000*g* for 10 min and supernatant protein extract was separated by SDS-PAGE, and transferred to a nitrocellulose membrane (GE Healthcare Amersham). Anti-GFP (1:3000; Invitrogen), anti-Tub (Agrisera, 1:5000), and anti-ATG8 (Agrisera, 1:5000) antibodies were used to probe the membrane. Quantification of the protein immunoblot signal was determined with the ImageJ software (10).

Microscopy

Confocal microscopy images of autophagosomes and ER structure were taken within the root elongation zone from GFP-ATG8e and GFP-HDEL seedlings, respectively. A Leica SP5 × MP confocal/multiphoton microscope system (Leica) was used with a 40x /1.4 oil immersion objective at the Iowa State University Roy J. Carver High Resolution Microscopy Facility (11). 7-day-old seedlings growing in MS were placed in liquid MS medium supplemented with 5µg/ml Tunicamycin (TM) for 6h and incubated or not for 1h with 200 µM NaHS, 200 µM ascorbic acid (ASC) or glutathione (GSH). Dimethyl sulfoxide (DMSO) was used as a solvent control for 6h and 1 µM concanamycin A for 6h where specified in figure 5. The number of autophagosomes in transgenic seedlings was counted and averaged from at least 15 images per sample.

Colocalization of YFP-ATG18a or YFP-ATG18a_C103S with Cerulean-ATG8e was analysed using a Leica TCS SP confocal microscope with a HCX PL APO CS 40X/1.25 oil immersion objective at the Cabimer facility (Seville, Spain). A sequential laser scan with cerulean and YFP was performed. 7-day-old seedlings growing in MS were placed in liquid MS medium supplemented with 5µg/ml Tunicamycin (TM) for 6h and incubated or not for 1h with 200 µM NaHS, using DMSO as solvent control. Six seconds interval time-lapse frames were photographed over 5 minutes, colocalization time and autophagosome size was analysed by ImageJ software (12) and the LOCI bio-formats ImageJ plugin. At least 150 autophagosomes were measured for each transgenic line, YFP-ATG18

x Cer-ATG8e and YFP-ATG18_C103S x Cer-ATG8e, to determine the average autophagosome size, and at least 15 images for each line to determine the average number of autophagosomes.

Excitation and emission wavelengths were 520 and 550 nm for YFP, 488 and 509 nm for GFP, and 450 and 475 nm for Cerulean.

bZIP60 splicing assay.

One-week-old seedlings growing in MS medium were transferred to liquid MS media and incubated with 5µg/ml Tunicamycin (TM) for 6, 12 and 24 hours and incubated or not for 1h with 200 µM NaHS. Total RNA was extracted using a plant RNeasy kit (Qiagen), and reverse-transcribed using the SuperScript™ III Reverse Transcriptase kit (Invitrogen) according to the manufacturers' instructions. RT-PCR was performed to detect bZIP60 mRNA splicing (13) with specific primers that cross the exon-exon boundary in the spliced RNA (SPS assay) using bZIP60F4/b60SB primers pair (Suppl. Table 1). Actin primers were used as a control.

*Expression and Purification of Free Glutathione S-transferase (*GST*) Protein.*

The complete complementary DNA of glutathione S-transferase (P08515) cloned into the pGEX-5X-1 vector (GE Life Sciences) was used to express free GST protein in *E.coli*. Transformed *E. coli* BL21 (DE3) cell cultures at an optical density at 600 nm of 0.6 were treated with 0.5 mM isopropyl-b-D-thiogalactopyranoside, and the cell cultures were incubated for 4 h at 30°C. Purification was performed by GST resin binding under non-denaturing conditions using the GST-Bind Kit (Novagen) according to the manufacturer's recommendations. Recombinant protein production and purification was assessed by SDS-PAGE using 10% (w/v) polyacrylamide gels and Coomassie Brilliant Blue staining. Purified protein was used in the PIP strips assay as a negative control and treated with increasing concentrations of Na_2S_4 to test persulfidation levels of free GST.

Figure legends

Fig. S1. Persulfidation level of free GST protein (A) and GST-ATG18a_C103S (B) expressed and purified from *E. coli* using the dimedone-switch method. Ratio of Cy5/Cl-NBF signals is used for the quantification and normalized band intensity is represented. Arrow indicates protein ATG18a_C103S band.

Fig. S2. (A) Immunoblot analysis using anti-GFP antibodies in protein extracts from pUBQ:GFP-ATG8 Arabidopsis seedlings treated with TM for 6, 12 and 24 hours and NaHS. Graph shows the relative band intensity. Bars represent means ± SD (n = 3).* $p < 0.05$. (B) bZIP60 mRNA splicing by RT-PCR analysis using specific primers to assay for spliced mRNA (SPS).

Fig. S3. ER degradation by autophagy in GFP-HDEL plants. (A) Quantification of ER-derived autophagic structures Bars represent means ± SD (n >10). Asterisks indicate statistically significant differences (ANOVA, Turkey Test, $p<0.05$) in comparison with their respective control treatment. (B-C) Immunoblot analysis using anti-ATG8 antibodies in protein extract from GFP-HDEL one week-old seedlings treated with TM for 6 hours and TM plus NaHS. Graph shows the relative band intensity and bars represent means ± SD (n = 3). Different letters indicate statistically significant differences (ANOVA, Turkey test, $p < 0.05$).

Fig. S4. GST tag does not affect GST-ATG18 binding to PIP strips. 0.5 µg of free GST protein was incubated with ± 200 µM NaHS, followed by incubation with PIP strips. Bound protein was detected using anti-GST primary antibody and anti-rabbit-HRP secondary antibody.

Fig. S5. Immunoblot of soluble and membrane-bound fractions of the fusion proteins YFP-ATG18a and YFP-ATG18a_C103S, obtained from transgenic lines treated with tunicamycin (TM) for 6 hours and sulfide (NaHS) for 1 hour

Fig. S6.- Confocal images for colocalization of YFP-ATG18a and YFP-ATG18a_C103S with Cer-ATG8e. Scale bars, 10 µm

Fig. S7.- Confocal images of the double transgenic plants YFP-ATG18a/Cer-ATG8e and YFP-ATG18a_C103S/Cer-ATG8e after treatment with TM and NaHS. Scale bars, 15 µm.

Fig. S8.- Immunoblot analysis of ATG8 in YFP-ATG18a and YFP-ATG18a_C103S seedlings after treatment with TM and sulfide (A-B) and under Nitrogen starvation and sulfide (C-D). (B) Relative band intensity quantification of ATG8. Bars represent means SD (n=3). Different letters indicate statistically significant differences (ANOVA, Turkey Test, $p<0.05$). (D) Relative band intensity quantification of ratio free CFP/CFP-ATG8. Bars represent means SD (n=3). Asterisks indicate statistically significant differences (ANOVA, Turkey Test, $p<0.05$) in comparison with their respective control treatment.

Fig. S9. Simulation of surface electrostatic potential distribution performed in (A) HsWIPI3 complex protein (PDB ID: 6KRL) and (B) AtATG18a 3D structural model. The structural elements of both proteins represented in cartoon form are superimposed with surface electrostatic potential. The cysteine 103 of AtATG18a is represented with spheres. The long flexible loop around the lipid binding site in AtATG18a is marked with an arrow. Positively and negatively charged regions are depicted in blue and red, respectively.

SI References

1. Xiong Y, Contento AL, Nguyen PQ, & Bassham DC (2007) Degradation of oxidized proteins by autophagy during oxidative stress in Arabidopsis. *Plant Physiol* 143(1):291-299.
2. Batoko H, Zheng HQ, Hawes C, & Moore I (2000) A rab1 GTPase is required for transport between the endoplasmic reticulum and golgi apparatus and for normal golgi movement in plants. *The Plant cell* 12(11):2201-2218.
3. Nolan TM, *et al.* (2017) Selective Autophagy of BES1 Mediated by DSK2 Balances Plant Growth and Survival. *Developmental cell* 41(1):33-46.e37.
4. Coll NS, *et al.* (2014) The plant metacaspase AtMC1 in pathogen-triggered programmed cell death and aging: functional linkage with autophagy. *Cell Death Differ* 21(9):1399-1408.
5. Clough SJ & Bent AF (1998) Floral dip: a simplified method for Agrobacterium - mediated transformation of Arabidopsis thaliana. 16(6):735-743.
6. Sali A & Blundell TL (1993) Comparative protein modelling by satisfaction of spatial restraints. *J. Mol. Biol.* 234(3):779-815.
7. Sato A, *et al.* (2009) Threonine at position 306 of the KAT1 potassium channel is essential for channel activity and is a target site for ABA-activated SnRK2/OST1/SnRK2.6 protein kinase. *Biochem. J.* 424(3):439-448.
8. Álvarez C, *et al.* (2011) Inhibition of Arabidopsis O-Acetylserine(thiol)lyase A1 by Tyrosine Nitration. *Journal of Biological Chemistry* 286(1):578-586.
9. Pardo JM & Serrano R (1989) Structure of a Plasma Membrane H+-ATPase Gene from the Plant Arabidopsis thaliana. *Journal of Biological Chemistry* 264(15):8557-8562.
10. Gallo-Oller G, Ordoñez R, & Dotor J (2018) A new background subtraction method for Western blot densitometry band quantification through image analysis software. *Journal of Immunological Methods* 457:1-5.
11. Pu Y & Bassham DC (2016) Detection of Autophagy in Plants by Fluorescence Microscopy. *Methods in molecular biology (Clifton, N.J.)* 1450:161-172.
12. Schneider CA, Rasband WS, & Eliceiri KW (2012) NIH Image to ImageJ: 25 years of image analysis. *Nature methods* 9(7):671-675.
13. Deng Y, *et al.* (2011) Heat induces the splicing by IRE1 of a mRNA encoding a transcription factor involved in the unfolded protein response in Arabidopsis. *Proceedings of the National Academy of Sciences of the United States of America* 108(17):7247-7252.

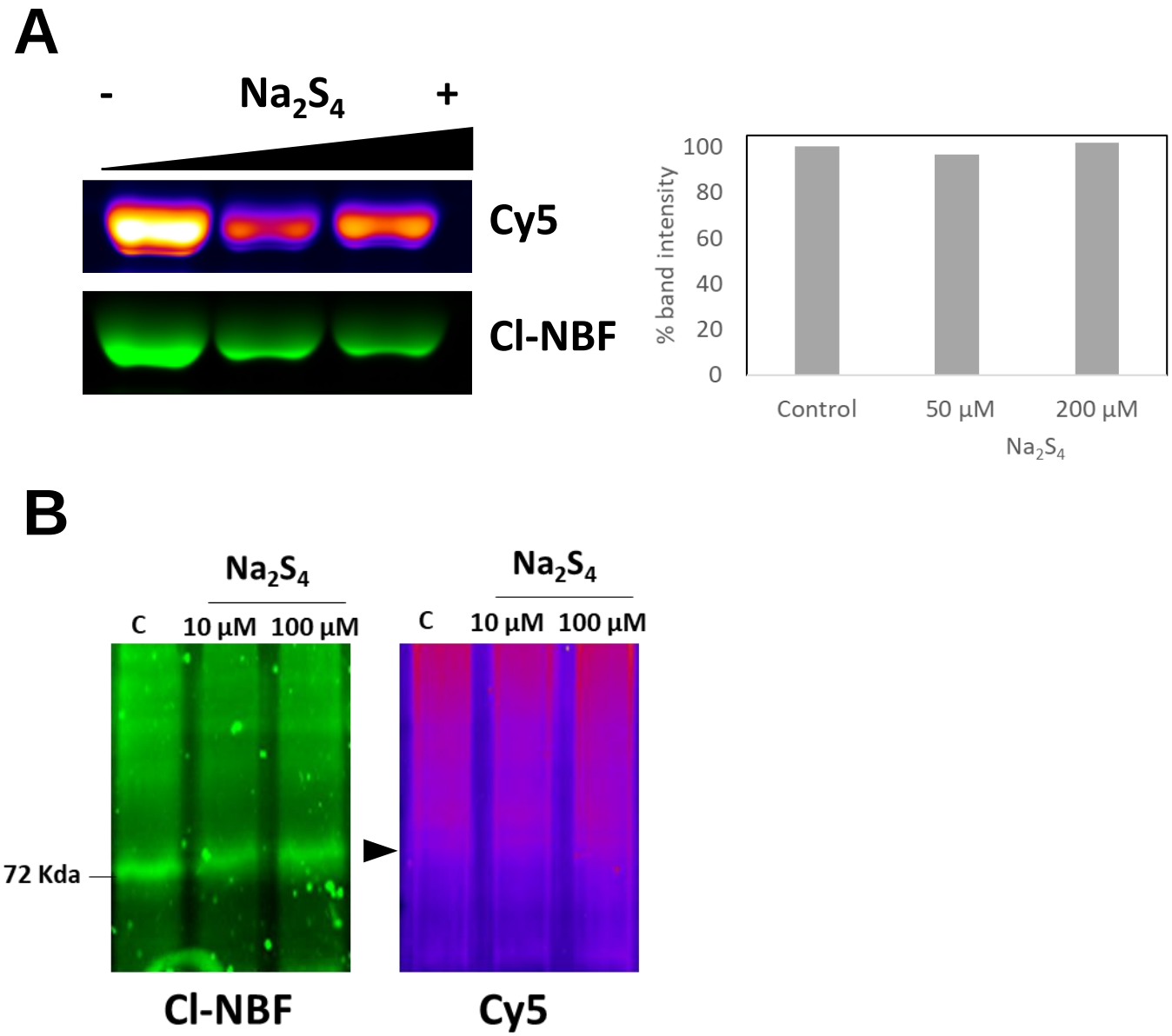

Fig. S1: Persulfidation level of free GST protein (A) and GST-ATG18a_C103S (B) expressed and purified from E. coli using dimedone-switch method. Ratio of Cy5/Cl-NBF signals is used for the quantification and normalized band intensity is represented. Arrow indicates protein ATG18a_C103S band.

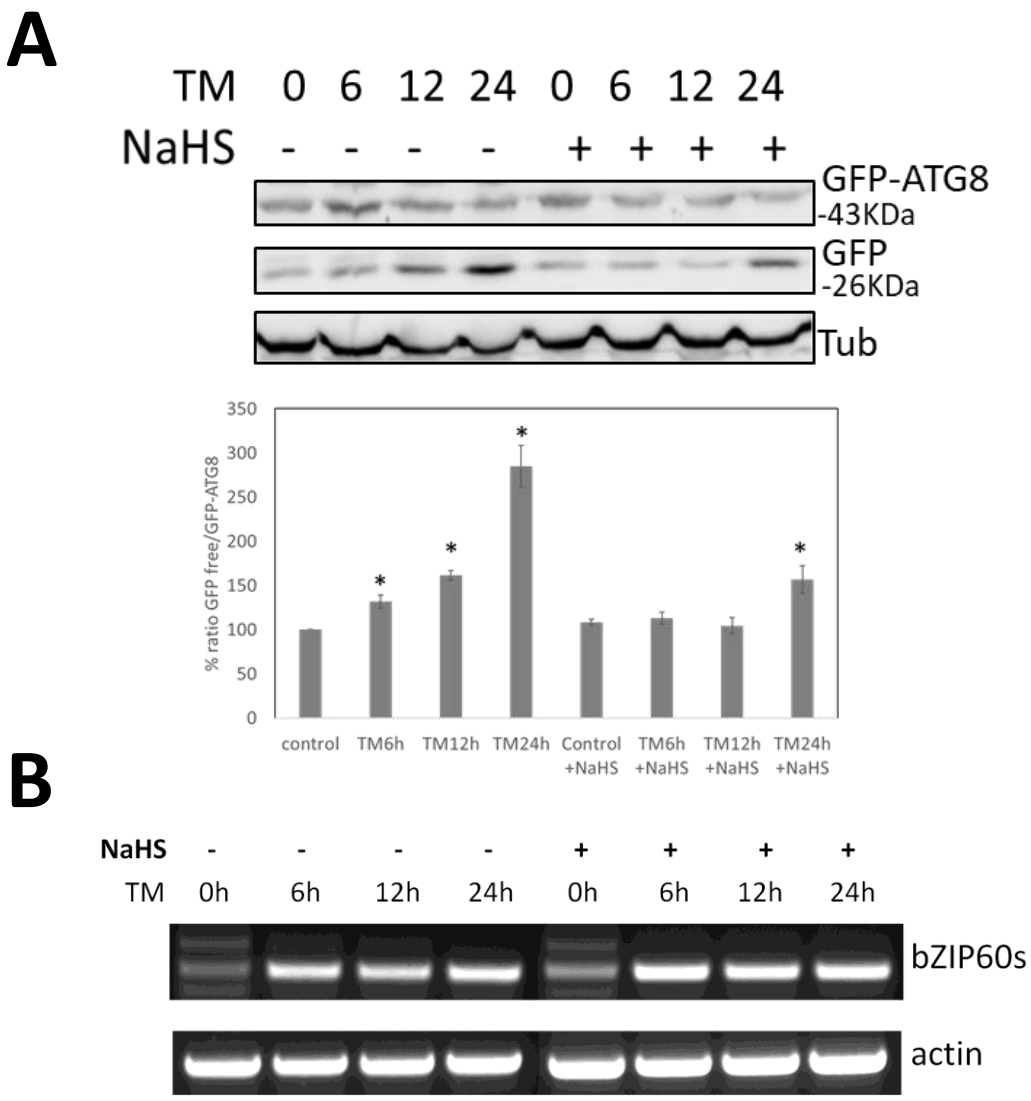

Fig. S2: (A) Immunoblot analysis using anti-GFP antibodies in protein extracts from pUBQ:GFP-ATG8 Arabidopsis seedlings treated with TM for 6, 12 and 24 hours and NaHS. Graph shows the relative band intensity. Bars represent means ± SD (n = 3).* $p < 0.05$.
(B) bZIP60 mRNA splicing by RT-PCR analysis using specific primers to assay for spliced mRNA (SPS).

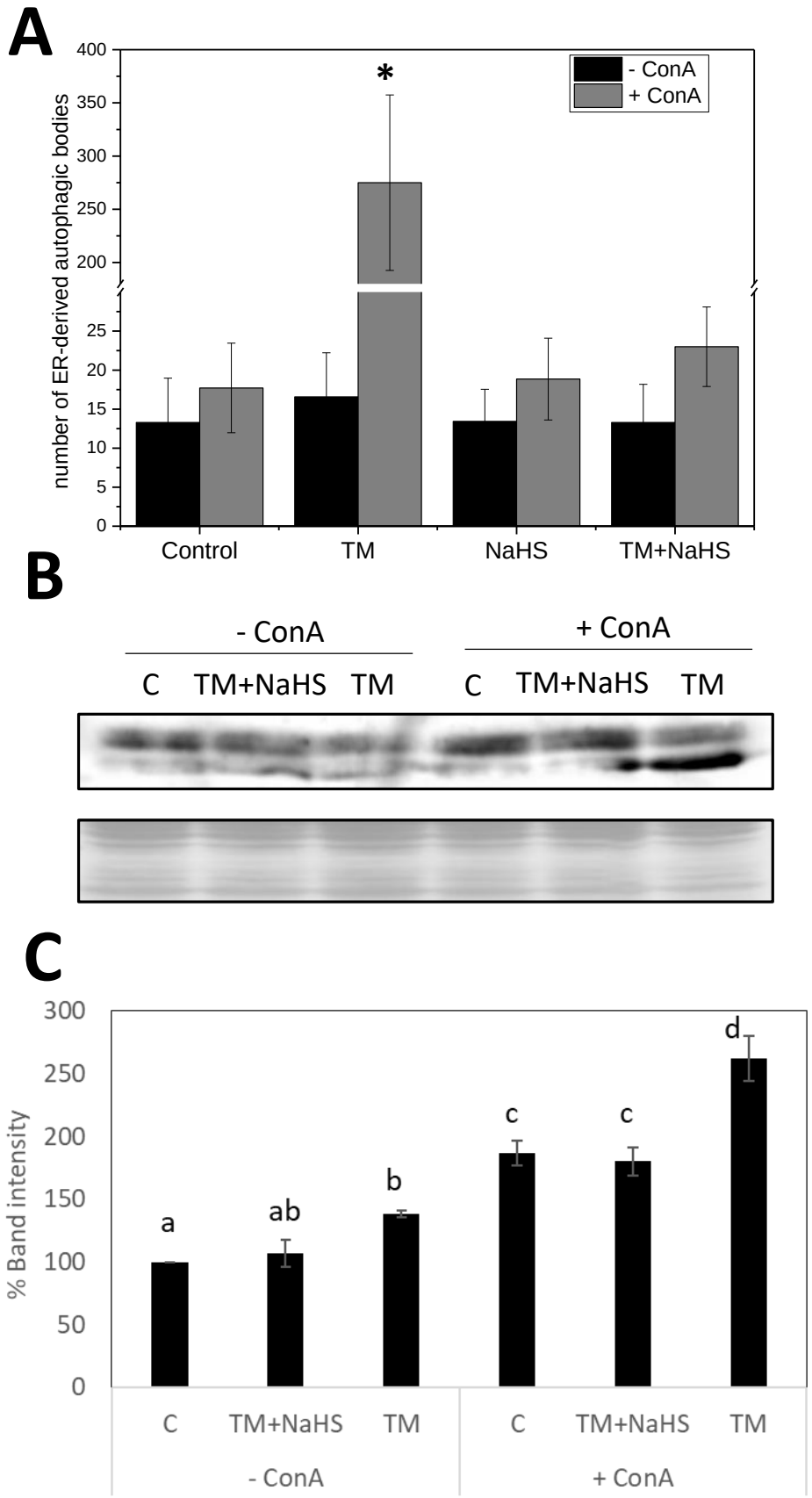

Fig. S3. ER degradation by autophagy in GFP-HDEL plants. (A) Quantification of ER-derived autophagic structures Bars represent means ± SD (n >10). Asterisks indicate statistically significant differences (ANOVA, Turkey Test, $p<0.05$) in comparison with their respective control treatment. (B-C) Immunoblot analysis using anti-ATG8 antibodies in protein extract from GFP-HDEL one week-old seedlings treated with TM for 6 hours and TM plus NaHS. Graph shows the relative band intensity and bars represent means ± SD (n = 3). Different letters indicate statistically significant differences (ANOVA, Turkey test, $p < 0.05$).

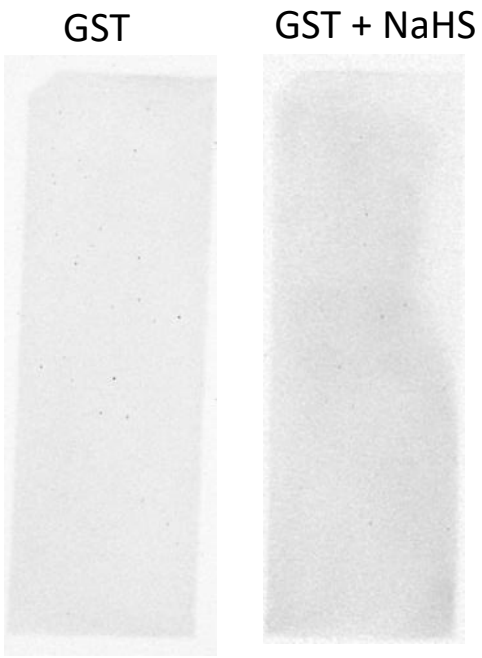

Fig. S4: GST tag does not affect GST-ATG18 binding to PIP strips. 0.5 µg of free GST protein was incubated with ± 200 µM NaHS, followed by incubation with PIP strips. Bound protein was detected using anti-GST primary antibody and anti-rabbit-HRP secondary antibody.

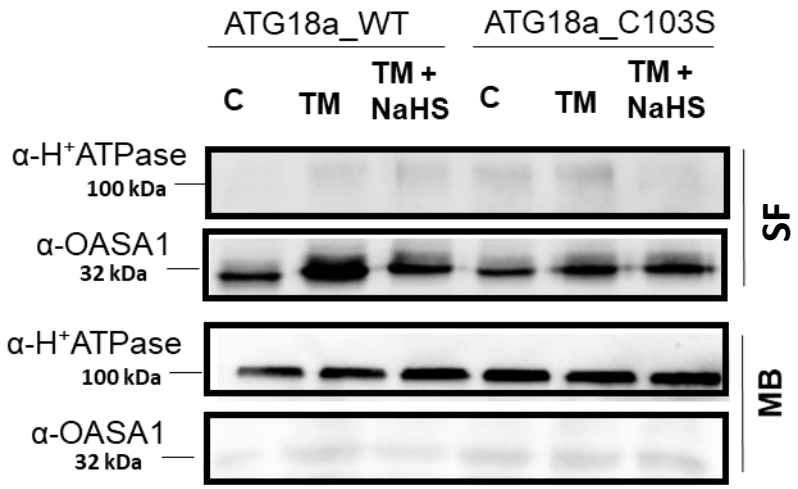

Fig. S5: Immunoblot of soluble (SF) and membrane-bound (MB) fractions of the fusion proteins YFP-ATG18a and YFP-ATG18a_C103S, obtained from transgenic lines treated with tunicamycin (TM) for 6 hours and sulfide (NaHS) for 1 hour.

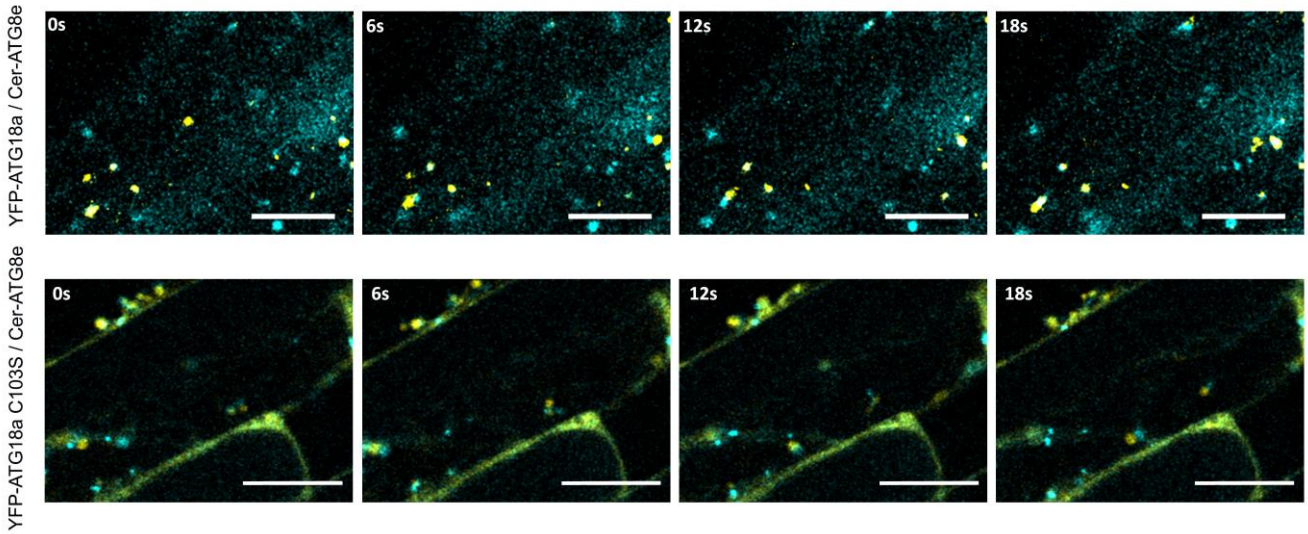

Fig. S6.- Confocal images for colocalization of YFP-ATG18a and YFP-ATG18a_C103S with Cer-ATG8e. Scale bars, 10 μm.

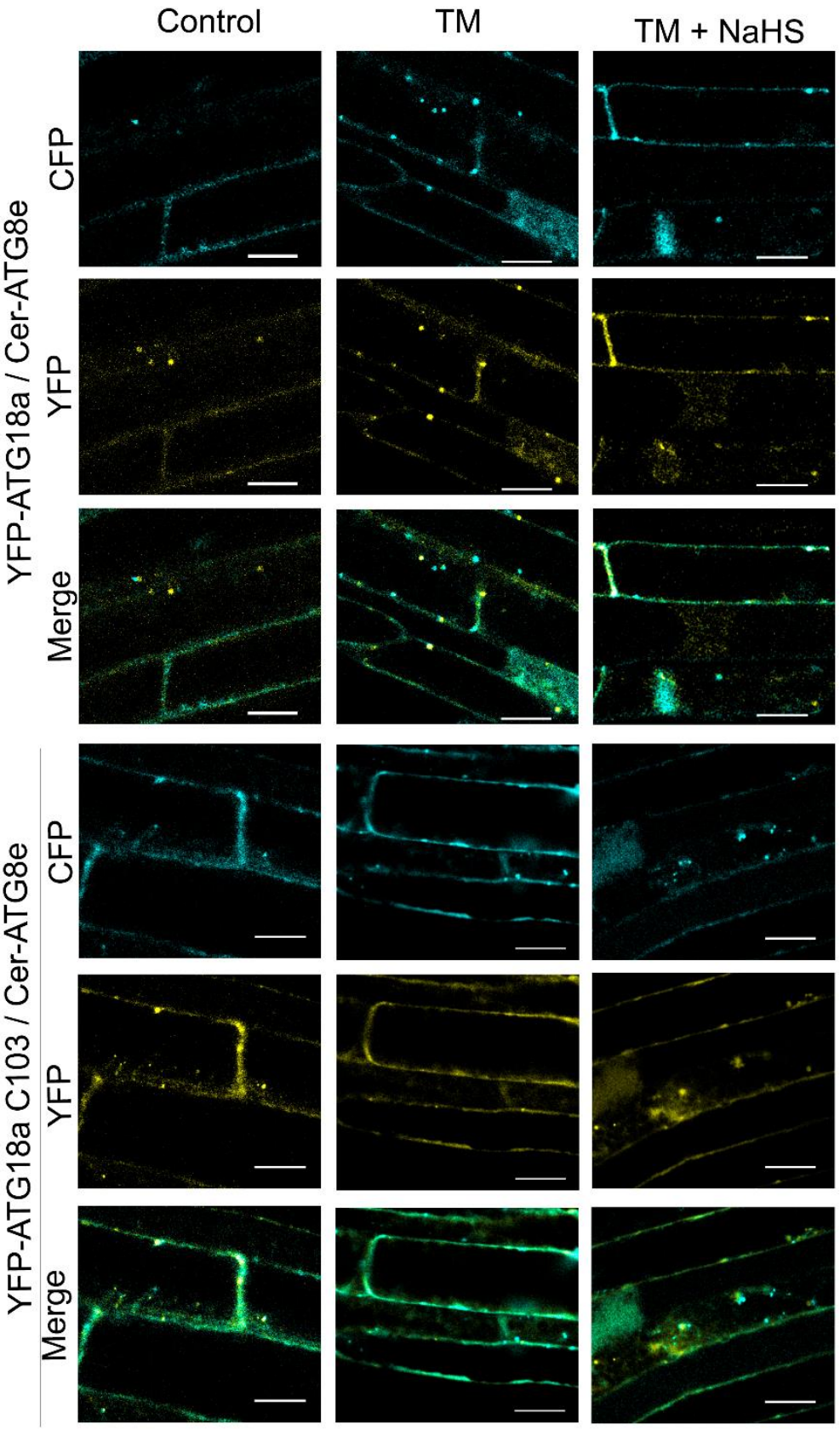

Fig.S7.- Confocal images of the double transgenic plants YFP-ATG18a/Cer-ATG8e and YFP-ATG18a_C103S/Cer-ATG8e after treatment with TM and NaHS. Scale bars, 15 μm.

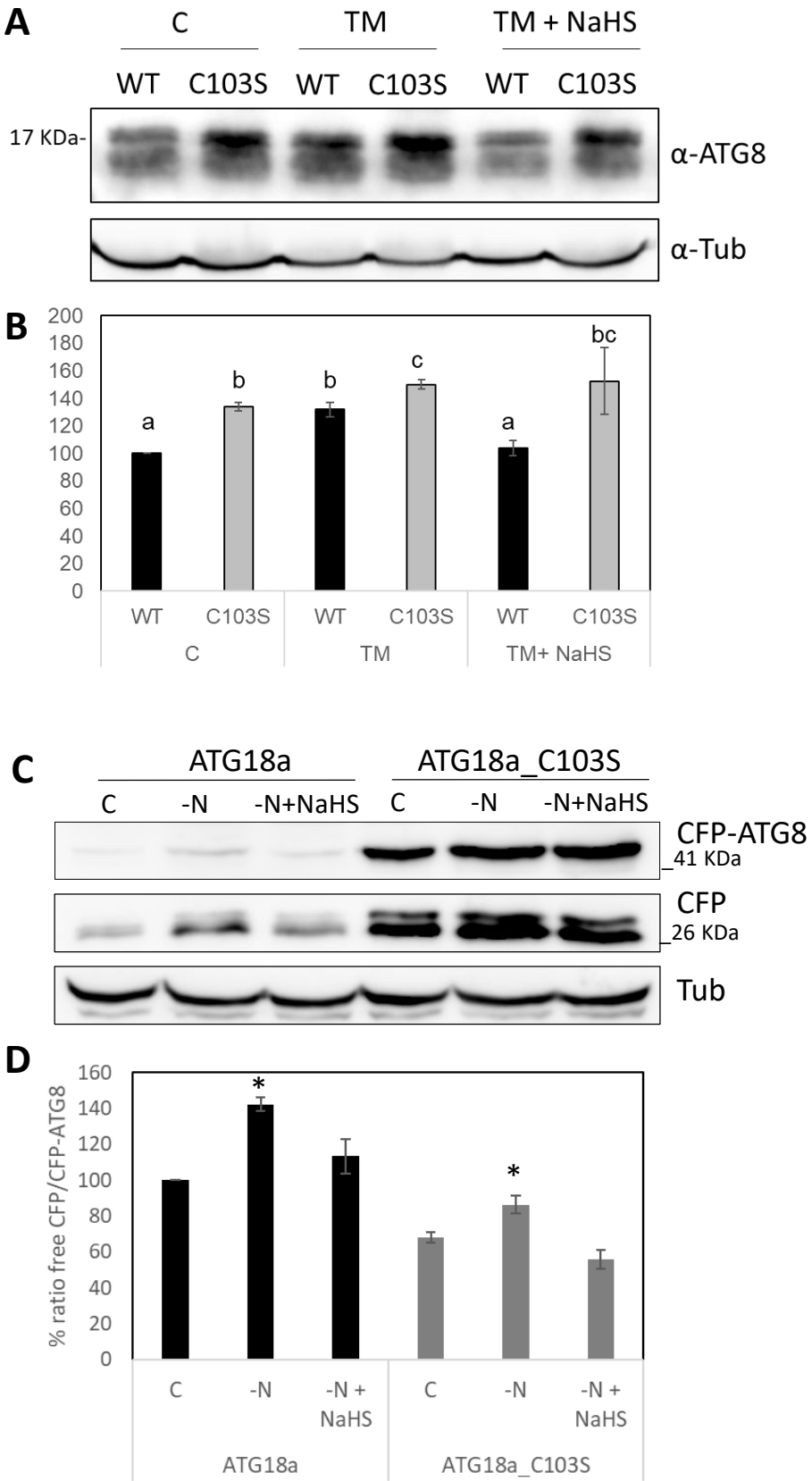

Fig. S8.- Immunoblot analysis of ATG8 in YFP-ATG18a and YFP-ATG18a_C103S seedlings after treatment with TM and sulfide (A-B) and under Nitrogen starvation and sulfide (C-D). (B) Relative band intensity quantification of ATG8. Bars represent means SD (n=3). Different letters indicate statistically significant differences (ANOVA, Turkey Test, $p<0.05$). (D) Relative band intensity quantification of ratio free CFP/CFP-ATG8. Bars represent means SD (n=3). Asterisks indicate statistically significant differences (ANOVA, Turkey Test, $p<0.05$) in comparison with their respective control treatment.

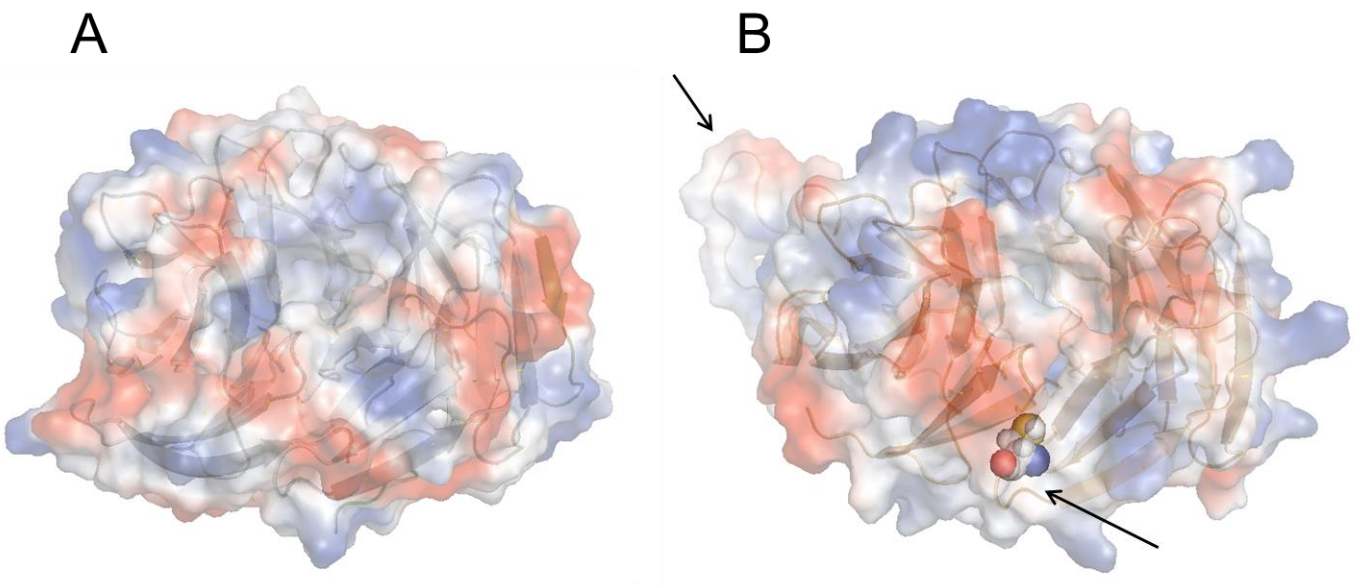

Fig. S9.- Simulation of surface electrostatic potential distribution performed in (A) HsWIPI3 complex protein (PDB ID: 6KRL) and (B) AtATG18a 3D structural model. The structural elements of both proteins represented in cartoon form are superimposed with surface electrostatic potential. The cysteine 103 of AtATG18a is represented with spheres. The long flexible loop around the lipid binding site in AtATG18a is marked with an arrow. Positively and negatively charged regions are depicted in blue and red, respectively.

Supplemental Table 1: The primers used in this paper.

Gene name	primer name	Primer sequences (5'-3')
bZIP60	bZIP60F4 (F)	GAAGGAGACGATGATGCTGTGG
bZIP60	b60SB2 (R)	AGCAGGGAACCCAACAGCAGACT
Actin	Actin (F)	GTTGGGATGAACCAGAAGGA
Actin	Actin (R)	GAACCACCGATCCAGACACT
ATG18a	C103S (F)	TCCGATCCCTTTCGCGAGAT
ATG18a	C103S (R)	GGAATTAAGGATCCGGAAGCCA